International Journal of Secondary Metabolite
2026, Vol. 13, No. 3, 760–788
https://doi.org/10.21448/ijsm.1791584
Journal homepage: https://dergipark.org.tr/en/pub/ijsm
Research Article

In vitro and bioinformatics evaluation of *Origanum vulgare* oil against *Acinetobacter baumannii* proteins

Gizem Köprülülü Kücük[1*], Tuğba Kaman[2], Ahmed Badri Abed[3], Safiye Elif Korcan[4], Muhsin Konuk[5]

[1]Istanbul Sisli Vocational School, Department of Radiotherapy, Istanbul, Türkiye
[2]Uskudar University, Vocational School of Health Services, Medical and Aromatic Plants, Istanbul, Türkiye
[3]Usak University, Department of Molecular Biology and Genetics, Faculty of Arts and Sciences, Usak, Türkiye
[4]Usak University, Usak Health Training School, Usak, Türkiye
[5]Uskudar University, Molecular Biology and Genetics, Faculty of Engineering and Natural Sciences, Istanbul, Türkiye

ARTICLE HISTORY

Received: Sep. 26, 2025
Accepted: Mar. 22, 2026

KEYWORDS

Molecular Docking,
Antibacterial Activity,
Pharmacophore,
Resistant Bacteria,
Plant-Based Compounds.

Abstract: *Acinetobacter baumannii* is a highly pathogenic, multidrug-resistant bacterium, posing a significant clinical challenge. Targeting key proteins such as OmpA and LigA offers potential for novel antimicrobial strategies. In this study, we evaluated the antimicrobial activity of *Origanum vulgare* essential oil against *A. baumannii* strains and investigated the mechanism by which the main components (carvacrol, beta-caryophyllene, gamma-terpinene, thymol, and p-cymene) in the supplement have an antimicrobial effect on *A. baumannii* using computational techniques. Amino acid sequences for OmpA and LigA were obtained from NCBI and modeled in 3D using Swiss-Model, AlphaFold, and GalaxyWeb. Ligands were sourced from PubChem, and models were evaluated with PROCHECK and ERRAT, while active binding sites were identified through Consurf analysis. Protein-ligand docking was performed using HDOCK and AutoDock Vina, with interactions analyzed via the PLIP tool. The MIC values for Origanum vulgare were determined following CLSI guidelines, using emulsified oils and bacterial inocula in 96-well plates, incubated at 37°C for 24 hours, with MIC defined as the lowest concentration showing no growth, measured at 450 nm absorbance. For OmpA, HDOCK identified thymol (-95.53) and carvacrol (-93.58) as the top-scoring ligands, whereas AutoDock Vina highlighted γ-terpinene (-5.6) and p-cymene (-5.4). For LigA, carvacrol (-112.21) and thymol (-111.73) showed the strongest HDOCK binding, while AutoDock Vina favored p-cymene (-7.0) and carvacrol (-6.9). The lowest MIC against the A13 strain was observed with a 1/64 dilution of Origanum vulgare oil, while 1/16 and 1/32 dilutions inhibited other strains. These results support the potential of these essential oils as antimicrobial agents.

INTRODUCTION

The World Health Organisation (WHO) has recently published a warning list of 12 bacteria that urgently need to be designed for new drugs. Carbapenem-resistant *Acinetobacter baumannii* ranks first on this list. According to the 2017 data of the Ministry of Health National Hospital Infections Surveillance Network (UHESA), *A. baumannii* ranks first in all healthcare-

*Corresponding Author: Gizem KOPRULULU KUCUK gzm0507@gmail.com Istanbul Sisli Vocational School, Department of Radiotherapy, Istanbul, Türkiye

The copyright of the published article belongs to its author under CC BY 4.0 license. To view a copy of this licence, visit http://creativecommons.org/licenses/by/4.0/

e-ISSN: 2148-6905

associated infections in Türkiye with a rate of 20.99%. It is also the bacterium that causes the most infections in pneumonia and ventilator-associated pneumonia, with rates of 35.6% and 44.4%, respectively. Today, this pathogen has become increasingly resistant to most antimicrobials, including broad-spectrum cephalosporins, penicillins, carbapenems, fluoroquinolones, and aminoglycosides (Smani *et al*.,2014). Therefore, there is an urgent need to research and develop effective solutions to combat resistance in *A. baumannii*. Carbapenems, colistin, tigecycline, and aminoglycosides are mostly preferred in the treatment of infections caused by *A. baumannii*. However, isolates may become resistant to the antibiotics used (Pogue *et al*., 2019). There is an urgent need to research and develop effective solutions to combat resistance in *A. baumannii*.

OmpA and LigA are important targets in terms of pathogenesis and resistance mechanisms in *A. baumannii*. Therapeutic approaches targeting these proteins may offer the following: i) Reduction of virulence (OmpA inhibition), ii) Impairment of genetic stability and DNA repair (LigA inhibition), iii) Increased efficacy of traditional antibiotics. A study showed that OmpA plays a role in the antimicrobial resistance phenotype of *A. baumannii* (Smani *et al*.,2014). However, the role of OmpA in antimicrobial resistance is still poorly understood. Antimicrobial agents targeting OmpA and LigA proteins are important areas of research to develop new strategies for the treatment of bacterial infections. Since these proteins play critical roles in supporting vital processes in bacteria, it is aimed to control bacterial infections by developing specific inhibitors or anti-binding molecules.

Outer membrane protein A (OmpA) is a multifunctional protein that plays a critical role in Gram-negative bacteria by maintaining cell envelope integrity and contributing to host cell adhesion, biofilm formation, and antibiotic resistance. In *Acinetobacter baumannii*, OmpA has been shown to be directly involved in virulence, cellular invasion, and mechanisms of immune evasion (Nie *et al*., 2020). Membrane-embedded OmpA contributes to multiple pathogenic traits, including resistance to antibiotics and serum-mediated killing, as well as biofilm development and host-pathogen interactions (Iyer *et al.*, 2017; Skerniškytė *et al.*, 2019; Mortensen *et al.*, 2012). OmpA has been reported to promote multiple pathogenic processes, including the induction of host cell apoptosis, biofilm development, systemic dissemination, and interactions with epithelial cells, primarily through its ability to bind host fibronectin (Ayoub Moubareck & Hammoudi Halat, 2020; Smani *et al*., 2012). In addition to its surface-associated functions, OmpA can be secreted within outer membrane vesicles, enabling its delivery into host cells. Once internalized, OmpA has been shown to target host cell mitochondria, where it induces mitochondrial dysfunction characterized by fragmentation and the subsequent release of cytochrome C, ultimately triggering apoptotic pathways (Tiku *et al.*, 2021). DNA ligases catalyze DNA strand ligation in replication and repair. Bacterial NAD^+-dependent DNA ligases (LigA) are essential in many bacteria and distinct from eukaryotic ligases**,** making them attractive antibacterial targets (Mills *et al*., 2011). Studies on LigA inhibition have demonstrated that suppression of this enzyme disrupts bacterial viability and highlights LigA as a promising antibacterial target with significant therapeutic potential (Meier *et al.*, 2008; Mills *et al.*, 2011; Alomari *et al.*, 2021).

In this context, the biological activities of specific plant-derived compounds have garnered significant attention for their potential to address such challenges. The use of natural compounds from different plants as antibacterial agents is an important strategy to discover bioactive products that could become useful therapeutic tools. This approach is particularly relevant in the context of pathogenic strains that are naturally tolerant to antibiotics, making them challenging to treat. Essential oils (EOs) or volatile compounds extracted from aromatic plants have been reported as remarkable antibacterial bioactive compounds with various mechanisms of action. Indeed, they act by disrupting membrane integrity and permeability, affecting proteins, disrupting cell membranes and respiratory processes, inhibiting biofilm formation, and disrupting quorum-sensing communication (Radi *et al.*, 2022).

Origanum vulgare L. essential oil (OVEO) contains monoterpenes, sesquiterpene hydrocarbons, and phenolic compounds (Fikry *et al.*, 2010). Their beneficial effects on antioxidant, anti-inflammatory, antitumor, and antimicrobial (antibacterial, antifungal, and antiparasitic) and skin disorders, as well as antihyperglycaemic and anti-Alzheimer activities, have been reported and confirmed in numerous studies (Lombrea *et al.*, 2020; Li *et al*., 2025; Simirgiotis *et al.*, 2020; Avola *et al*., 2020). Although a study reported that terpenes are effective agents against *A. baumannii* biofilms and that essential oils may offer promising ways to develop new strategies to prevent infections and overcome antibiotic resistance (Tapia-Rodriguez *et al.*, 2023) studies on the antimicrobial action mechanism of different fatty acids on *A. baumannii* are needed. Today, molecular docking is an important tool in drug discovery and development. This technique is used to predict the binding affinity and binding mechanism of a molecule to a target protein (Meng *et al*., 2011).

In this study, the antimicrobial activity of high-content carvacrol, beta-caryophyllene, gamma-terpinene, thymol, and p-cymene essential oil extract of *O.vulgare* against *A. baumannii* strains was evaluated, and the mechanism was elucidated using computational techniques.

METHOD

SwissADME and ADMET Properties

The SwissADME web tool enables the calculation of basic physicochemical, pharmacokinetic, drug-like, and related parameters for one or more molecules (https://www.swissadme.ch/).

Pass online prediction of biological activity and side effects

PASS Online (Prediction of Activity Spectra for Substances) functions as a freely accessible web resource for the prediction of biological activity spectra. This resource is designed for the prediction of biological activity spectra of organic compounds based on their structural formulae for more than 4000 biological activity types with an average accuracy of over 95% (http://www.way2drug.com/passonline). It obtains an output information as a list of predicted activity types with the predicted probability of 'being active' Pa and 'being inactive' Pi for each activity type, and these probabilities range from zero to one. The chance of experimentally finding a given activity increases with increasing Pa and decreasing Pi. It is reported that the chance of finding an experimental activity is quite high when $Pa > 0.7$, the chance of detecting an experimental activity is lower in the range $0.5 < Pa < 0.7$, and the chance of detecting an experimental activity is even lower for $Pi < Pa < 0.5$ (Filimonov *et al*., 2014).

Protein Sequence Obtaining

The amino acid sequences of LigA and OmpA from Acinetobacter baumannii, obtained from NCBI in FASTA format (https://www.ncbi.nlm.nih.gov), along with their 3D structures modeled using Swiss-Model, GalaxyWEB, and AlphaFold (Waterhouse *et al*., 2018; Ko *et al*., 2012; Jumper *et al*., 2021), and ligands (carvacrol, beta-caryophyllene, gamma-terpinene, thymol, and p-cymene) sourced from PubChem are presented in Table 1.

Table 1. Amino acid sequences of LigA and OmpA from *Acinetobacter baumannii* (https://pubchem.ncbi.nlm.nih.gov/).

LigA from *Acinetobacter baumannii* amino acid sequence
MAITSVIEQMRQLIQLIAKHNHAYYVMDQPTISDSEYDHLFHQLKALEEQYPELVQADSPTT
KVGGQALSKFESVTHVVPMLSLGNVFNQEDLFAFARRVEERLPNQKVQYEVELKLDGLAIS
LWYENGVLVRGVTRGDGETGEDITQNVKTIRNLPKVLHSEKYEIPRLLEVRGEVLMPKSGFE
KLNADQEAKGEKTFANPRNAAAGSLRQLDPNIAAARPLAFYAYGIAQCEPNHGLTTMHDSL
QWLTELGFQIAERQYLCNSIQEVQQRYEQIQQERPNLQVEIDGMVVKVDDLKQQQQLGFLS
REPRWATAYKFPAQAALTTVEQIDWQVGRTGTLTPVARLNPVFVGGVTVSNVTLHNIGEIH
RLDVRIGDTVSVYRTGDVIPKVEKVWPEFRPAEAEVVHLPESCPVCASPVVMPEGEALARCS
GGLYCAAQRIEAIRHFVSRKAMDIEGLGDRWVESLLRLDLLKDVADIYHLHEHRETLLGIEK

MGEKSVQNLIDAIEASKKTTLARFIYALGIRGVGETTARMLANTFQTLEALKAANVEALKKT PDVGDITAEWIADFFLAPHNIEVLDRLIAAGIHWDAPTAPTRQPLNGESWVLTGTLEQMTRD QATQMLQALGARVSGSVSSKTKCVVAGEKAGSKLEKAAKLGIPVMNETDFLSLMAGYGQT LS
OmpA from *Acinetobacter baumannii* amino acid sequence
MKLSRIALATMLVAAPLAAANAGVTVTPLLLGYTFQDSQHNNGGKDGNLTNSPELQDDLF VGAALGIELTPWLGFEAEYNQVKGDVDGASAGAEYKQKQINGNFYVTSDLITKNYDSKIKP YVLLGAGHYKYDFDGVNRGTRGTSEEGTLGNAGVGAFWRLNDALSLRTEARATYNADEEF WNYTALAGLNVVLGGHLKPAAPVVEVAPVEPTPVAPQPQELTEDLNMELRVFFDTNKSNIK DQYKPEIAKVAEKLSEYPNATARIEGHTDNTGPRKLNERLSLARANSVKSALVNEYNVDAS RLSTQGFAWDQPIADNKTKEGRAMNRRVFATITGSRTVVVQPGQEAAAPAAAQ

Homology Modeling and Quality Assessment of Models

Homology modeling was performed using Swiss Model, AlphaFold, and GalaxyWeb (Waterhouse *et al*., 2018; Ko *et al*., 2012; Jumper *et al*., 2021) based on amino acid sequences of OmpA and LigA obtained from NCBI (https://www.ncbi.nlm.nih.gov). Models were built using templates selected by GMQE, sequence identity, and Ramachandran plots (Jumper *et al*., 2021), and their quality was assessed with SAVES v0.6 using ERRAT and PROCHECK (https://saves.mbi.ucla.edu). The analyses confirmed favorable stereochemical compatibility and reliable atomic interactions, ensuring high-quality models for further study.

Detection of The Active Sites of Proteins

Hydrophilic and hydrophobic regions of OmpA and LigA were identified using UCSF Chimera version 1.15 (Colovos *et al*., 1993), highlighting their roles in protein stability and function. Conserved regions and potential active or ligand-binding sites were analyzed with the Consurf web server, which evaluates evolutionary conservation by comparing homologous sequences from various species (Armon *et al*., 2001). This analysis revealed functionally significant regions critical for biological activity and protein interactions, providing insights into the proteins' roles.

Docking Performance and Selection of Ideal Model

Docking studies using AutoDock Vina and HDOCK analyzed the interactions of OmpA and LigA with ligands such as thymol, carvacrol, and beta-caryophyllene (Trott *et al*., 2010; Yan *et al*., 2020). Protein-ligand complexes were prepared in UCSF Chimera, and docking models were selected based on scores and visualized for interactions such as hydrogen bonds and hydrophobic contacts (Pettersen *et al*., 2004). The grid box was manually defined to encompass the predicted binding pocket of the OmpA protein, with center coordinates set to x = 23, y = 6, and z = -21, and grid dimensions of 10 × 10 × 10 Å. For LigA, the grid box was similarly positioned to cover the predicted active site, with center coordinates of x = -13, y = -13, and z = 26, and grid dimensions of 12 × 12 × 12 Å. This analysis revealed key residues and molecular mechanisms driving protein-ligand interactions. Docking models were further analyzed using the PLIP (Protein-Ligand Interaction Profiler) tool to identify detailed interaction profiles. PLIP automatically detected binding types such as hydrogen bonds, π-π stacking, salt bridges, and hydrophobic interactions, enhancing the characterization of binding sites (https://plip-tool.biotec.tu-dresden.de/plip-web/plip/index).

Determination of MIC of Essential Oils

We evaluated the bactericidal properties of two essential oils. We purchased essential oils of oregano, *Origanum vulgare,* from Orlife Global, Istanbul / Türkiye. The oil is high-quality natural oil (carvacrol, beta-caryophyllene, gamma-terpinene, thymol, and p-cymene) that is free of artificial additives. This study included four isolates of *A. baumannii*. *A.baumannii* OR792201, OR792202, OR792203, and OR792204 were the four isolates that were determined

by genotypic identification. Due to the hydrophobic nature of essential oils, we used water-based bacterial solutions to create homogeneous micelles (Man *et al*., 2019). Eppendorf microcentrifuge tubes were used to create suspensions with two millilitres of each essential oil and sterile water (1:1). For 20 minutes at room temperature (around 25°C), a sonicated water bath (Ultrasons-HD, also known as JP SELECTA in Spain) was used to create micelles. The bottom homogenous opalescent phase was used as a stock micelle solution and extracted using small, sterile pipette tips. The MIC of essential oils using broth microdilution was determined in accordance with the Clinical and Laboratory Standards Institute (CLSI) standards (Clinical and Laboratory Standards Institute, 2012). In the MIC experiments, wells containing bacterial inoculum without essential oil were used as positive growth controls, whereas wells containing only the culture medium and the emulsified solvent system without bacteria were used as negative controls. The bacterial inocula's turbidity was adjusted to 0.5 McFarland. 50 microlitres of diluted bacterial suspension and 50 microlitres of diluted essential oil were added to each well of a 96-well plate. Then, twofold serial dilutions were performed. Plates were incubated for 24 hours at 37°C. The MIC value was defined as the lowest concentration at which the isolates under investigation did not exhibit any symptoms of growth. Every test was conducted three times. The absorbance at 570 nm was recorded in order to provide standard readings for MIC (Nadeem *et al*., 2021; Erol *et al*., 2021). Thermo Scientific TMMultiskanTM FC-Filter-based Microplate Photometer, manufactured by Thermo Fisher Scientific Incorporated (USA), was used to take the reading.

RESULTS

Pharmacokinetic and Drug-Like Evaluation of Selected Bioactive Compounds Using SwissADME Drug similarity involves the assessment of the compatibility between the physicochemical properties of a drug and the desired biopharmaceutical properties in the human body. Lipinski's five rules serve as important criteria for assessing drug similarity by imposing certain conditions that determine whether a drug is a suitable candidate. Considering these properties and filters, the physicochemical properties of the selected bioactive molecules (carvacrol, thymol, p-cymene, gamma-terpinene, and beta -caryophyllene) are presented in Table 2, lipophilicity and water solubility in Table 3, Pharmacokinetic properties in Table 4, and Drug-Like Properties in Table 5.

SwissAdme results showed that carvacrol, p-cymene, gamma-terpinene, and thymol were moderately lipophilic with log Po/values of 2.82, 3.50, 3.35, and 2.80, respectively; these four components exhibited good water solubility and high gastrointestinal absorption and passed through the blood-brain barrier. Beta-caryophyllene has been shown to exhibit good/moderate water solubility with a log Po/value (4.24) less than 5, low gastrointestinal absorption, and does not pass through the blood-brain barrier. Carvacrol, p-cymene, and thymol passed Lipinski, Veber, Egan, PAINS, and Brenk filters but not Ghose and Muegge filters. γ-Terpinene passed Lipinski, Veber, Egan, PAINS filters; beta-caryophyllene passed Lipinski, Ghose, Veber, Egan, PAINS filters. Thymol and carvacrol inhibited liver enzymes CYP1A2, p-cymene inhibited CYP2D6, and beta-caryophyllene inhibited CYP2C19 and CYP2C9 enzymes and did not inhibit/affect other enzymes. The synthetic accessibility value of carvacrol, p-cymene, gamma-terpinene, and thymol was 1. The closer this value is to 1, the easier it can be synthesized, and the closer it is to 10, the more difficult it is to synthesize. The synthetic accessibility value of beta-caryophyllene was 4.51 (Table 3 and Table 4).

Table 2. Lipophilicity and water solubility properties of selected bioactive compounds calculated by SwissADME Tools (https://www.swissadme.ch/).

	Lipophilicity	Water Solubility					
	Consensus Log Po/w	Log S (ESOL)	Solubility Class	Log S (Ali)	Solubility Class	Log S (SILICOS-IT)	Solubility Class
Carvacrol	2.82	-3.31	Soluble	-3.60	Soluble	-3.01	Soluble
P-cymene	3.50	-3.63	Soluble	-3.81	Soluble	-3.57	Soluble
Gamma-terpinene	3.35	-3.45	Soluble	-4.22	Moderately soluble	-2.23	Soluble
Thymol	2.80	-3.19	Soluble	-3.40	Soluble	-3.01	Soluble
Beta-caryophyllene	4.24	-3.87	Soluble	-4.10	Moderately soluble	-3.77	Soluble

Table 3. Pharmacokinetics of selected bioactive compounds by SwissADME Tools (https://www.swissadme.ch/).

	GI absorption	BBB permission	P-gp substrate	CYP1A2 inhibitors	CYP2C19 inhibitors	CYP2C9 inhibitors	CYP2D6 inhibitors	CYP3A4 inhibitors	Log Kp (skin permeation) (cm/s)
Carvacrol	High	Yes	No	Yes	No	No	No	No	-4.74 cm/s
P-cymene	Low	Yes	No	No	No	No	Yes	No	-4.21 cm/s
Gamma-terpinene	Low	Yes	No	No	No	No	No	No	-3.94 cm/s
Thymol	High	Yes	No	Yes	No	No	No	No	-4.87 cm/s
Beta-caryophyllene	Low	No	No	No	Yes	Yes	No	No	-4.44 cm/s

Table 4. Drug-likeness properties and Medicinal chemistry of selected active compounds by SwissADME Tools (https://www.swissadme.ch/).

	Drug likeness rules						Medicinal chemistry			
	Lipinski	Ghose	Veber	Egan	Muegge	Bioavailability Score	PAINS	Brenk	Lead likeness	Synthetic Accessibility
Carvacrol	Yes; 0 violation	No, 1 violation MW<160	Yes	Yes	No; 2 violations: MW<200, Heteroatoms<2	0.55	0 alert	0 alert	No; 1 violation: MW<250	1.00
P-cymene	Yes; 1 violation: MLOGP>4.15	No; 1 violation: MW<160	Yes	Yes	No; 2 violations: MW<200, Heteroatoms<2	0.55	0 alert	0 alert	No; 2 violations: MW<250, XLOGP3>3.5	1.00
Gamma-terpinene	Yes; 0 violation	No; 1 violation: MW<160	Yes	Yes	No; 2 violations: MW<200, Heteroatoms<2	0.55	0 alert	1 alert: isolated _alkene	No; 2 violations: MW<250, XLOGP3>3.5	3.11
Thymol	Yes; 0 violation	No, 1 violation MW<160	Yes	Yes	No; 2 violations: MW<200, Heteroatoms<2	0.55	0 alert	0 alert	No; 1 violation: MW<250	1.00
Beta-caryophyllene	Yes; 1 violation: MLOGP>4.15	Yes	Yes	Yes	No; 1 violation: Heteroatoms<2	0.55	0 alert	1 alert: isolated _alkene	No; 2 violations: MW<250, XLOGP3>3.5	4.51

Table 5. Prediction activities for the selected compounds were generated using the PASS online server (http://www.way2drug.com/passonline).

	Carvacrol		P-cymene		Gamma-terpinene		Thymol		Beta-caryophyllene	
Biological Activity	Pa	Pi	Pa	Pi	Pa	Pi	Pa	Pi	Pa	Pi
Antiseptic	0.824	0.004	0.573	0.009	-	-	0.913	0.003	-	-
Antieczematic	0.811	0.016	0.884	0.006	0.854	0.009	0.788	0.021	0.897	0.005
Antiseborrheic	0.810	0.017	0.830	0.013	0.685	0.040	0.846	0.011	0.335	0.111
Antiinfective	0.784	0.005	0.623	0.011	0.367	0.060	0.829	0.005	-	-
Antiinflammatory	0.674	0.019	0.644	0.024	0.470	0.066	0.549	0.044	0.745	0.011
Antipruritic	0.549	0.024	0.555	0.023	0.428	0.050	0.431	0.009	0.442	0.047
Skin irritation, inactive	0.506	0.015	0.401	0.026	0.240	0.063	0.437	0.022	0.219	0.072
Antipsoriatic	0.501	0.023	0.417	0.040	0.346	0.057	0.438	0.035	0.734	0.005
Dermatologic	0.489	0.034	0.428	0.047	0.447	0.043	0.491	0.034	0.734	0.006
Photosensitizer	0.379	0.014	0.383	0.013	0.339	0.029	0.379	0.014	-	-
Antioxidant	0.302	0.023	0.144	0.110	-	-	0.299	0.023	0.174	0.075
Wound healing agent	0.254	0.075	0.312	0.043	0.235	0.087	0.259	0.071	0.166	0.165
Possible Adverse & Toxic Effects										
Irritation	0.880	0.004	0.622	0.011	0.810	0.004	0.863	0.004	0.788	0.005
Allergic contact dermatitis	0.790	0.007	0.759	0.011	0.452	0.074	0.766	0.010	-	-
Skin irritation, moderate	0.771	0.004	0.633	0.005	0.438	0.010	0.666	0.005	0.115	0.047
Skin irritation, corrasive	0.661	0.006	0.770	0.004	0.591	0.008	0.805	0.004	-	-
Allergic dermatitis	0.658	0.018	0.594	0.032	0.383	0.107	0.766	0.010	-	-
Skin irritative effect	0.599	0.009	0.512	0.013	0.523	0.013	0.599	0.009	0.163	0.056
Dermatitis	0.616	0.058	0.551	0.079	0.480	0.104	0.603	0.061	0.279	0.240
Skin irritation, weak	0.491	0.009	0.473	0.010	0.479	0.010	0.511	0.009	0.178	0.044
Skin irritation, high	0.348	0.021	0.298	0.024	0.222	0.038	0.345	0.021	0.154	0.054

*Pa: active probability Pi: inactive probability

PASS Online Prediction of Biological and Skin-Related Properties

The selected bioactives were screened with SMILES codes obtained from the PubChem database15, and after the screening, the biological activity of five phytochemical compounds (carvacrol, p-cymene, gamma-terpinene, thymol, and beta-caryophyllene) for various dermatological conditions was focused, and the data presented on the activity on the skin were filtered and shown in Table 5.

Table 6 shows that thymol and carvacrol showed high activity in terms of antiseptic and antiinfective activity, beta-caryophyllene showed high activity in terms of anti-eczematic, antipsoriatic, anti-inflammatory, and dermatological activity, and p-cymene showed high activity in terms of antiseborrheic activity. In terms of antipruritic activity, it can be interpreted that all components exhibit moderate activity, and in terms of skin irritation inactivity, beta-caryophyllene shows the lowest activity among the selected compounds, and carvacrol shows higher activity than the others.

Homology Modeling and Quality Assessment of LigA and OmpA

Five LigA homology models were generated using Swiss-Model, and model selection was performed based on established structural quality criteria, including GMQE score, sequence identity, and stereochemical validation metrics. Among the generated models**,** B0V8E4.1.A was selected as the final LigA model because it consistently outperformed the alternative candidates across all primary evaluation parameters**.** The data supporting this selection are presented in Table 7. The ideal model for LigA, B0V8E4.1.A, was selected for its high GMQE value (0.89) and 100% sequence identity, ensuring strong structural accuracy. Generated using Swiss-Model and AlphaFold, this model offers insights into LigA's structural features and potential functions (Table 6).

Table 6. Assessment of LigA templates with GMQE and sequence identity (Waterhouse *et al*., 2018).

Template	GMQE	Seq Identity
B0V8E4.1.A	0.89	100%
5tt5.1.A	0.77	52.03%
2owo.1.D	0.76	52.18%
1dgs.2.A	0.67	44.76%

AlphaFold assigns a pLDDT confidence score (0–100) to each residue, with scores above 50 indicating reliable structures14. Five LigA models were generated using GalaxyWeb, which improved template selection with HHsearch rescoring and evaluated secondary structures using PsiPred and DSSP13. Comparative analyses of model confidence and structural features are detailed in Tables 7 and 8.

Table 7. Homology modeling of LigA from *Acinetobacter baumannii* (Waterhouse *et al.*, 2018; Jumper *et al*., 2021).

Swiss MODEL (GMQE: 0.89)	AlphaFold
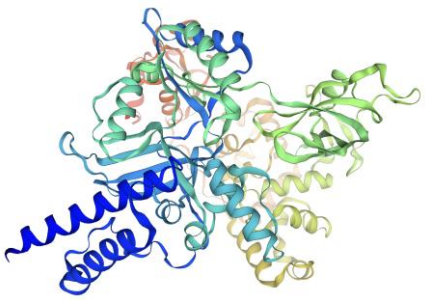	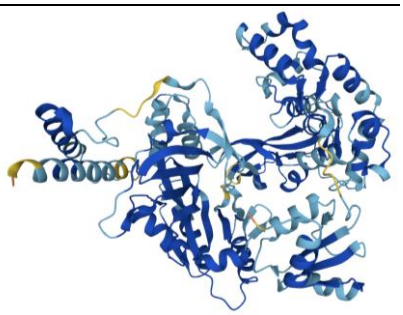

Table 8. GlaxyWEB modeling results of LigA (Ko *et al*., 2012).

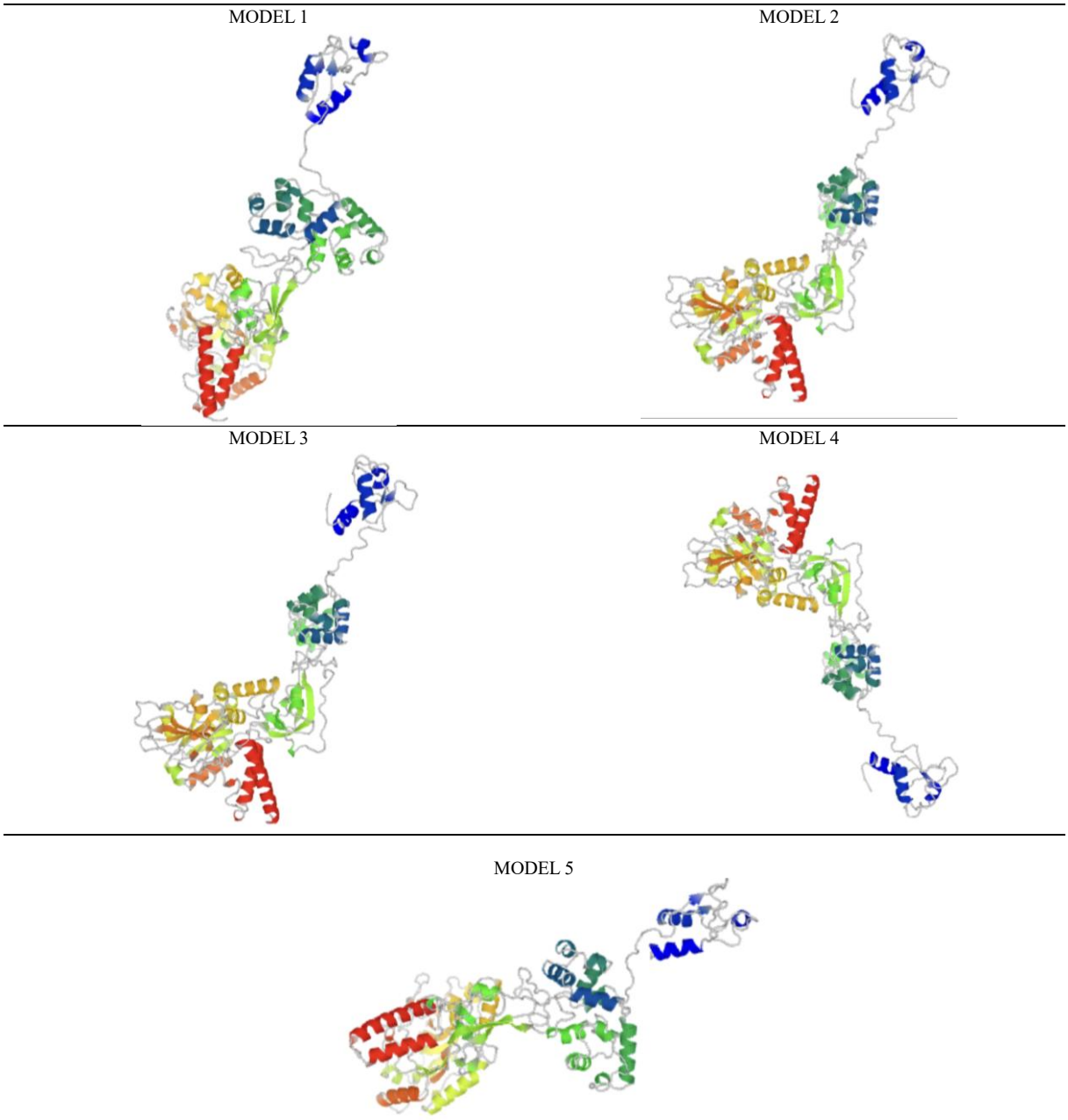

Complementary structure prediction using AlphaFold further supported this selection, as the corresponding AlphaFold model demonstrated high per-residue confidence scores (pLDDT > 50 for the majority of residues), confirming the robustness of the predicted fold (Table 6). GalaxyWeb modeling provided additional refinement and reliability assessment by identifying Unreliable Local Regions (ULRs). While ULRs were detected in regions 1–7, 159–168, and 231–240, the remaining regions, including ULR 3 (591–594) and ULR 5 (481–491), were classified as sufficiently reliable, supporting the overall structural integrity of the model (Table 9).

Table 9. ULR results of LigA (Ko *et al*., 2012).

No	Start	End	Refined
1	1	7	YES
2	159	168	YES
3	591	594	NO
4	231	240	YES
5	481	491	NO

A similar selection strategy was applied for OmpA modeling. Although the 3td5.3.B template showed 100% sequence identity, its lower GMQE score indicated reduced overall reliability, leading to its exclusion. Instead, the A3M8K2.1.A template, with a GMQE of 0.85 and 99.44% sequence identity, was selected as the most suitable template, balancing alignment accuracy and model quality (Table 10).

Table 10. Assessment of OmpA templates with GMQE and sequence identity (Ko *et al.*, 2012).

Templates	GMQE	Sequence Identity
7q5c.1.A	0.12	14.29%
2mlh.1.A	0.13	13.04%
3nb3.1.A	0.24	22.43%
3td5.3.B	0.28	100.00%
A3M8K2.1.A	0.85	99.44%

Table 11 details the outcomes of OmpA modeling by Swiss Model and AlphaFold, offering insights into its structural features, functions, and interactions.

Table 11. Homology modeling of OmpA (Ko *et al*., 2012; Jumper *et al.*, 2021).

Swiss MODEL (GMQE: 0.85) AlphaFold

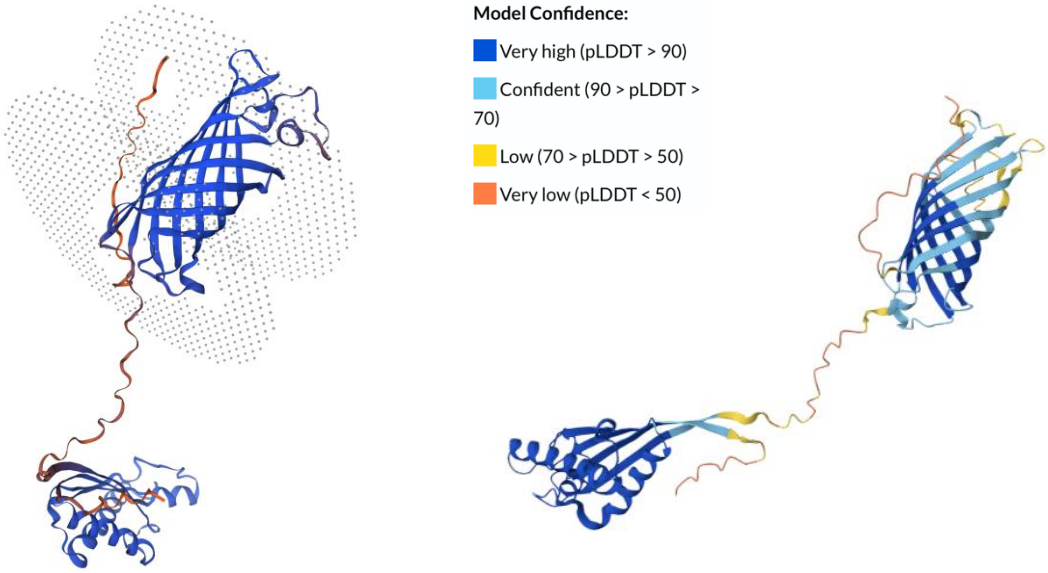

Table 12. GlaxyWEB modeling results of OmpA (Ko *et al.*, 2012)

MODEL 1 MODEL 2

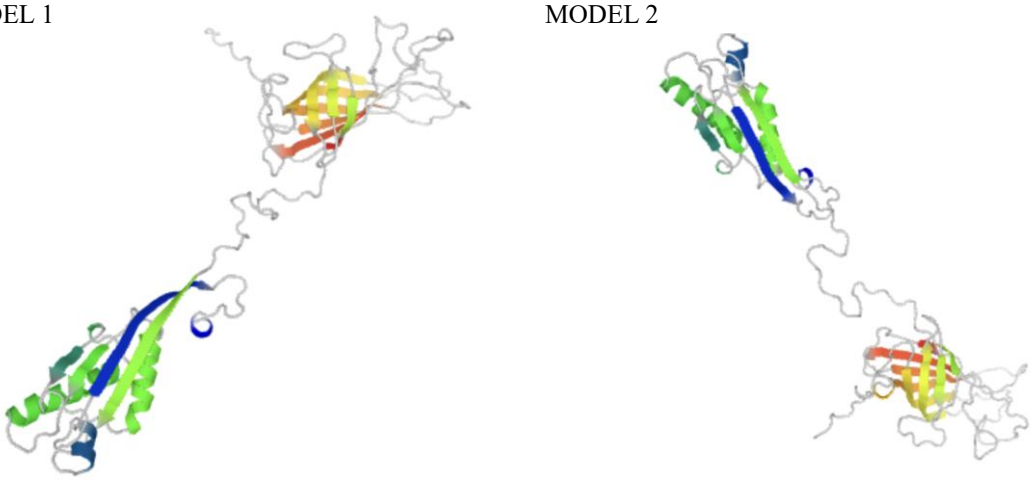

MODEL 3

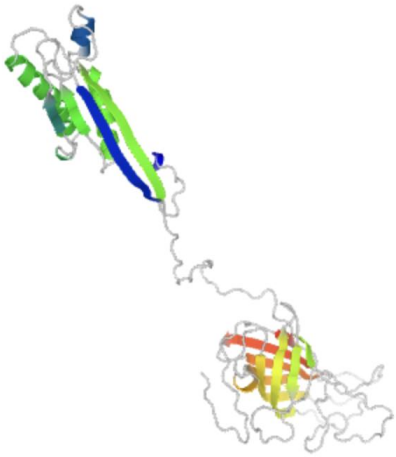

MODEL 4



MODEL 5

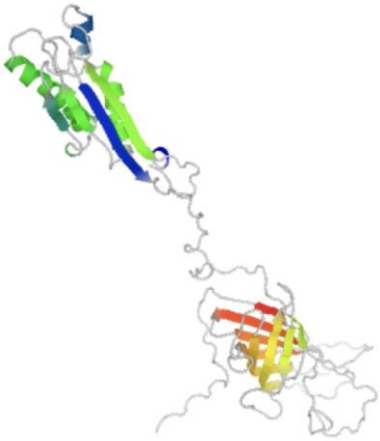

Five models generated using GalaxyWeb are presented in Table 12, with comparisons made to evaluate the results. GalaxyWeb enhanced template selection through HHsearch rescoring, and secondary structure predictions from PsiPred were assessed using the DSSP tool for Model 1.

GalaxyWeb identified and improved Unreliable Local Regions (ULRs) in the protein, with ULR 1 (residues 339–356) and ULR 2 (residues 206–215) requiring further attention, while ULR 3 (residues 1–22) was considered sufficiently reliable, as shown in Table 13.

Table 13. ULR results of OmpA (Ko *et al.*, 2012).

No	Start	End	Refined
1	339	356	YES
2	206	215	YES
3	1	22	NO

The analysis indicates that the OmpA protein structure exhibits good stereochemical compatibility, with a high "core" percentage and low "disallowed" percentage in the Ramachandran plot, confirming its high accuracy and stability. The model quality assessment was performed by Saves v6.0, and the results were shown in Figures 1 and 2.

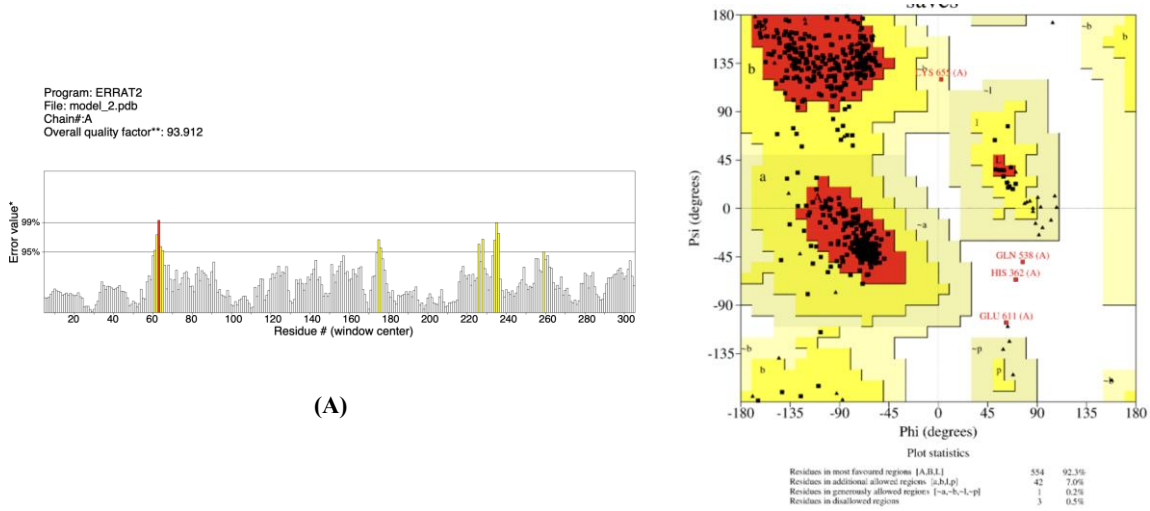

(A) (B)

Figure 1. Quality assessment of OmpA A) ERRAT value and B) Ramachandran plot (https://saves.mbi.ucla.edu).

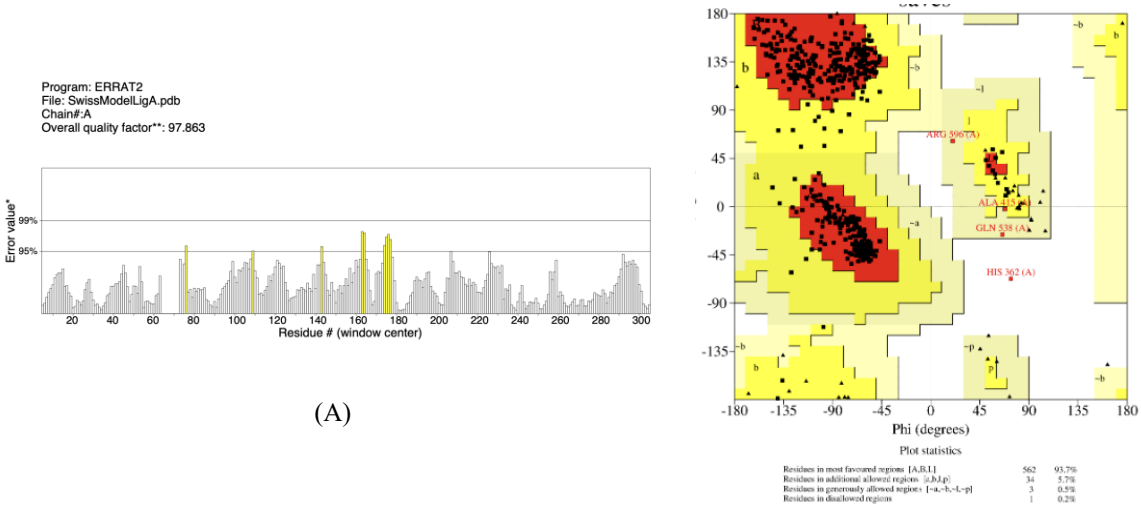

(A) (B)

Figure 2. Quality assessment of LigA A) ERRAT value and B) Ramachandran plot (https://saves.mbi.ucla.edu).

Final stereochemical validation using PROCHECK and ERRAT further confirmed the reliability of the selected models. Structural analyses of OmpA and LigA using PROCHECK and ERRAT revealed high-quality models, with OmpA showing a PROCHECK value of 92.3% and an ERRAT value of 93.91%, while LigA had a PROCHECK value of 93.7% and an ERRAT value of 97.86%, indicating strong stereochemical compatibility and stability for both proteins (Table 14).

Table 14. PROCHECK and ERRAT values of OmpA and LigA proteins (Structure Validation Services (https://saves.mbi.ucla.edu).

Protein Name	PROCHECK value		ERRAT value
	Favored region	Disallowed region	
OmpA	92.3%	0.5%	93.91%
LigA	93.7%	0.2%	97.86%

Docking Results

The docking process for OmpA and LigA with various ligands was conducted using AutoDock Vina (Trott and Olson 2010) and visualized with UCSF Chimera version 1.15 (Colovos *et al*., 1993), with results presented in Tables 15 and 16 for OmpA and LigA, respectively. Docking

studies of OmpA and LigA with ligands (carvacrol, p-cymene, thymol, gamma-terpinene, and beta-caryophyllene) were performed using AutoDock Vina and HDOCK. As a result of HDOCK analysis, thymol (-95.53), followed by carvacrol (-93.58) and p-cymene (-86.31) for OmpA and carvacrol (-112,21), thymol (-111, 73) and p-cymene (-97, 96) for LigA. In AutoDock Vina, gamma-terpinene exhibited a strong binding score of -5.6, along with p-cymene (-5.4) for OmpA and p-cymene (-7.0) and carvacrol (-6.9) for LigA. The ideal models were selected based on these negative docking scores. Details were shown in Tables 15, 16, 17, and 18 (Trott *et al*., 2010; Yan *et al*., 2020; Pettersen *et al*., 2004).

The differences observed between the HDOCK and AutoDock Vina results can be attributed to the distinct docking algorithms employed. While HDOCK primarily evaluates shape complementarity and surface matching, AutoDock Vina estimates binding free energies based on physicochemical interactions. Therefore, differences in ligand ranking between the two methods were observed. The combined use of both approaches in this study enables a more comprehensive evaluation of protein-ligand interactions. Although HDOCK was used to evaluate shape complementarity and binding site localization, AutoDock Vina results were primarily considered for model selection due to their ability to estimate binding free energies. Therefore, the most energetically favorable protein–ligand complexes identified by AutoDock Vina were selected as representative models.

Table 15. Comparison of docking results for OmpA (Trott *et al*., 2010; Yan *et al*., 2020; Pettersen *et al*., 2004; https://plip-tool.biotec.tu-dresden.de/plip-web/plip/index).

HDOCK OmpA- Beta-caryophyllene Docking score: -73.14	AutoDock Vina OmpA- Beta- caryophyllene Docking score: -3.4	2D protein–ligand interaction map
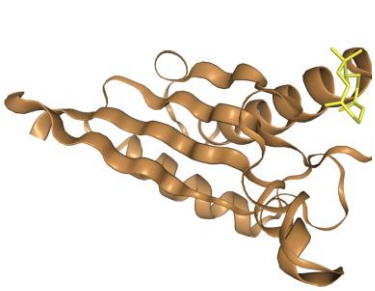	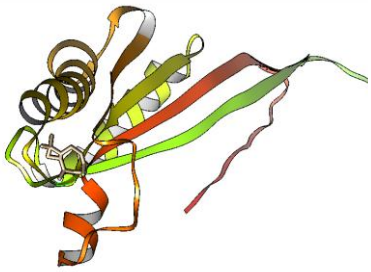	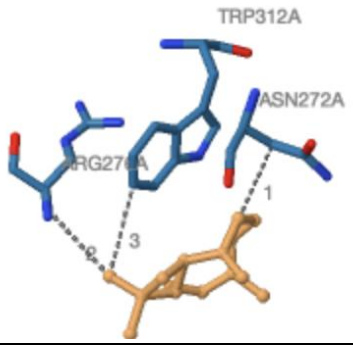
HDOCK OmpA- Carvacrol Docking score: -93.58	AutoDock Vina OmpA- Carvacrol Docking score: -5.1	2D protein–ligand interaction map
		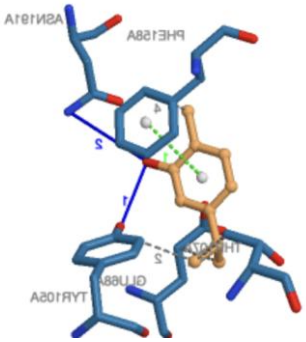
HDOCK OmpA- Gamma-terpinene Docking score: -85.37	AutoDock Vina OmpA- Gamma-terpinene Docking score: -5.6	2D protein–ligand interaction map



HDOCK
OmpA- P-cymene
Docking score: -86.31

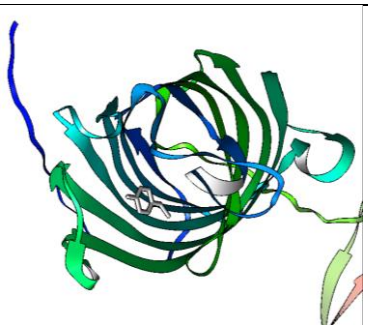

AutoDock Vina
OmpA- P-cymene
Docking score: -5.4

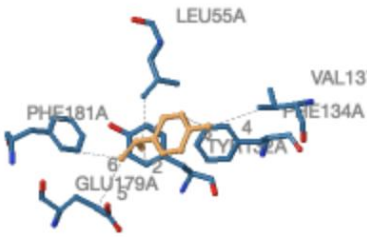

2D protein–ligand interaction map

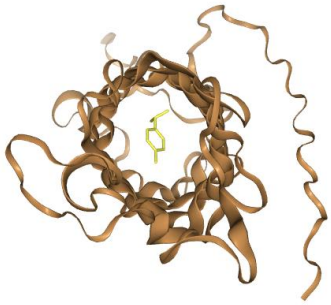

HDOCK
OmpA- Thymol
Docking score: -95.53

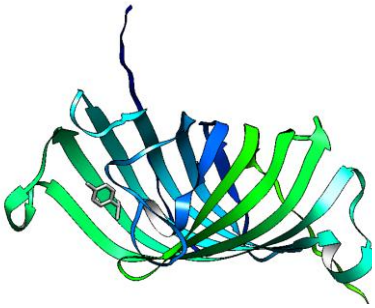

AutoDock Vina
OmpA- Thymol
Docking score: -4.6

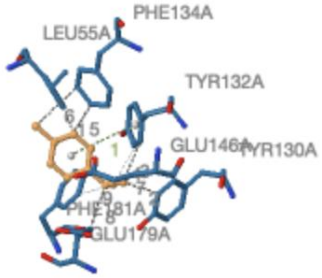

2D protein–ligand interaction map



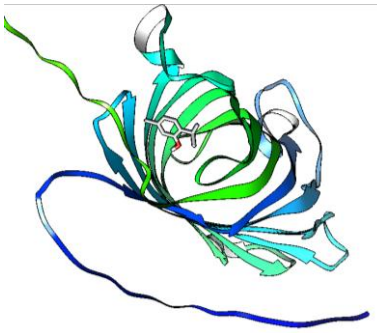

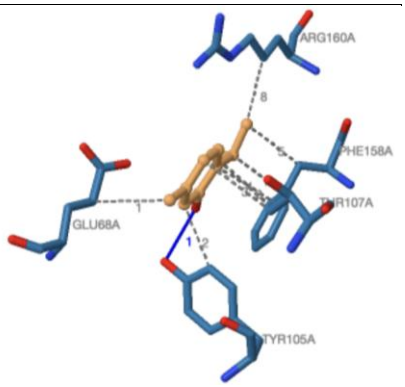

Table 16. Summary of HDOCK and AutoDock vina docking results for OmpA and ligands (Trott *et al*., 2010; Yan *et al*., 2020).

Results of HDOCK		Docking Score	Confidence Score	Ligand rmsd
OmpA-Beta-caryophyllene	Model 1	-73.14	0.1769	22.09
	Model 2	-72.75	0.1768	28.09
	Model 3	-66.83	0.1593	44.40
	Model 4	-65.90	0.1568	24.17
	Model 5	-65.38	0.1555	24.90
	Model 6	-62.05	0.1469	33.02
	Model 7	-61.12	0.1446	46.23
	Model 8	-60.32	0.1426	28.19
	Model 9	-58.80	0.1390	20.11
	Model 10	-57.48	0.1358	54.65
Results of AutoDock Vina		Docking Score	RMSD I.b	RMSD u.b
OmpA-Beta-caryophyllene	Model 1	-3.4	1.094	4.811
	Model 2	-3.3	1.414	4.152
	Model 3	-3.2	5.877	8.508

	Model 4	-3.2	1.362	4.927
	Model 5	-3.2	0.967	3.14
	Model 6	-3.1	1.63	4.957
	Model 7	-3.1	4.372	7.062
	Model 8	-3.1	1.596	3.664
Results of HDOCK		Docking Score	Confidence Score	Ligand rmsd
OmpA- Carvacrol	Model 1	-93.58	0.2445	12.09
	Model 2	-90.48	0.2332	29.68
	Model 3	-84.33	0.2119	31.91
	Model 4	-82.29	0.2052	20.06
	Model 5	-69.44	0.1664	33.69
	Model 6	-69.26	0.1659	14.31
	Model 7	-58.61	0.1385	20.36
	Model 8	-56.56	0.1337	13.86
	Model 9	-55.56	0.1314	19.95
	Model 10	-52.47	0.1245	21.96
Results of AutoDock Vina		Docking Score	RMSD I.b	RMSD u.b
OmpA- Carvacrol	Model 1	-5.1	2.101	4.682
	Model 2	-5.1	1.823	4.355
	Model 3	-3.6	1.411	2.023
	Model 4	-3.5	1.315	2.401
Results of HDOCK		Docking Score	Confidence Score	Ligand rmsd
OmpA-Gamma-terpinene	Model 1	-85.37	0.2154	28.56
	Model 2	-84.22	0.2116	13.39
	Model 3	-77.60	0.1903	31.07
	Model 4	-67.87	0.1621	19.81
	Model 5	-63.48	0.1505	30.83
	Model 6	-55.77	0.1319	35.19
	Model 7	-53.94	0.1277	23.31
	Model 8	-49.32	0.1178	18.96
	Model 9	-48.85	0.1168	19.57
	Model 10	-45.95	0.1110	21.50
Results of AutoDock Vina		Docking Score	RMSD I.b	RMSD u.b
OmpA-Gamma-terpinene	Model 1	-5.6	0.627	1.999
	Model 2	-5.3	2.384	4.356
	Model 3	-5.2	1.215	4.609
	Model 4	-5.2	1.788	3.713
	Model 5	-5.0	2.262	4.18
	Model 6	-5.0	2.925	5.165
	Model 7	-5.0	1.907	4.984
	Model 8	-4.9	2.068	5.353
Results of HDOCK		Docking Score	Confidence Score	Ligand rmsd
OmpA-P-cymene	Model 1	-86.31	0.2186	28.73
	Model 2	-82.09	0.2045	12.12
	Model 3	-78.55	0.1933	30.99
	Model 4	-70.28	0.1688	20.05
	Model 5	-63.61	0.1509	30.42
	Model 6	-61.48	0.1455	14.07
	Model 7	-56.41	0.1333	21.29
	Model 8	-55.56	0.1314	35.15
	Model 9	-52.39	0.1243	18.59
	Model 10	-51.49	0.1224	18.62

Results of AutoDock Vina		Docking Score	RMSD I.b	RMSD u.b
OmpA-P-cymene	Model 1	-5.8	0.023	1.534
	Model 2	-5.4	1.167	4.544
	Model 3	-5.4	1.238	4.517
	Model 4	-4.8	1.31	4.737
	Model 5	-4.8	1.813	4.355
	Model 6	-4.7	2.163	4.755
	Model 7	-4.7	2.73	4.814
	Model 8	-4.7	1.417	1.961
Results of HDOCK		Docking Score	Confidence Score	Ligand rmsd
OmpA-Thymol	Model 1	-95.53	0.2517	12.22
	Model 2	-88.00	0.2244	28.61
	Model 3	-80.81	0.2004	32.26
	Model 4	-74.77	0.1907	19.55
	Model 5	-76.40	0.1866	13.30
	Model 6	-73.78	0.1788	30.71
	Model 7	-63.20	0.1498	35.23
	Model 8	-62.44	0.1479	21.27
	Model 9	-61.89	0.1465	19.07
	Model 10	-53.81	0.1274	22.21
Results of AutoDock Vina		Docking Score	RMSD I.b	RMSD u.b
OmpA-Thymol	Model 1	-4.6	1.895	4.661
	Model 2	-4.5	10.81	11.948
	Model 3	-4.4	10.826	12.584
	Model 4	-4.1	10.906	12.596
	Model 5	-4.1	1.158	4.219
	Model 6	-4.1	11.014	11.971
	Model 7	-4.0	1.683	2.403
	Model 8	-3.8	11.336	12.778

Table 17. Comparison of docking results for LigA (Trott *et al*., 2010; Yan *et al*., 2020; Pettersen *et al*., 2004; https://plip-tool.biotec.tu-dresden.de/plip-web/plip/index).

HDOCK LigA- Beta-caryophyllene Docking score: -93.18	AutoDock Vina LigA- Beta- caryophyllene Docking score: -6.7	2D protein–ligand interaction map
	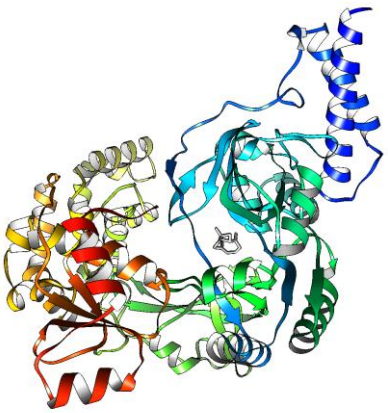	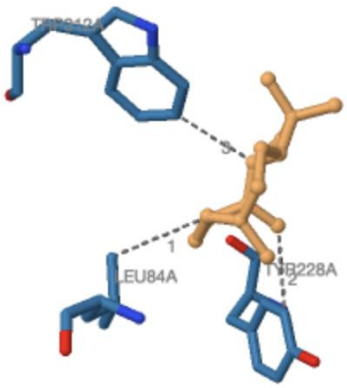

HDOCK LigA- Carvacrol Docking score: -112.21	AutoDock Vina LigA- Carvacrol Docking score: -6.9	2D protein–ligand interaction map
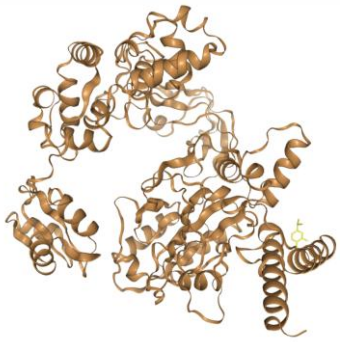	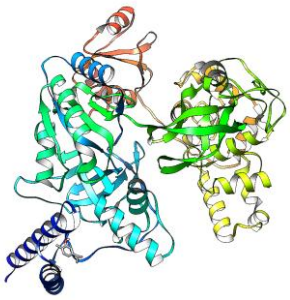	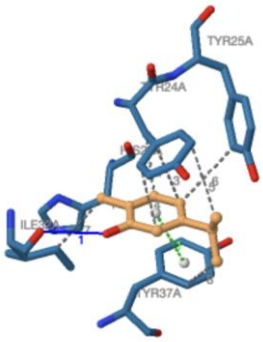
HDOCK LigA- Gamma-terpinene Docking score: -94.55	AutoDock Vina LigA- Gamma-terpinene Docking score: -6.7	2D protein–ligand interaction map
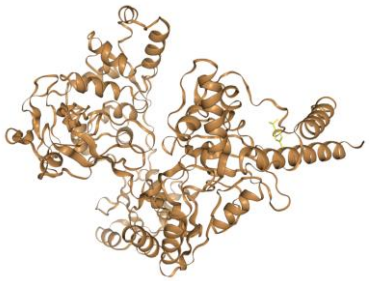	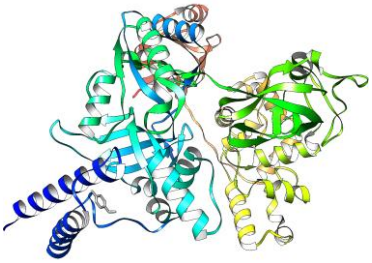	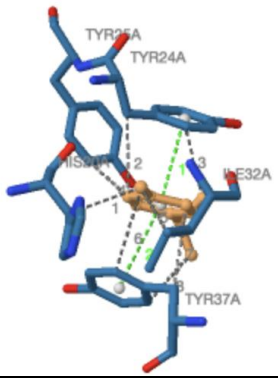
HDOCK LigA- P-cymene Docking score: -97.96	AutoDock Vina LigA- P-cymene Docking score: -7.0	2D protein–ligand interaction map
	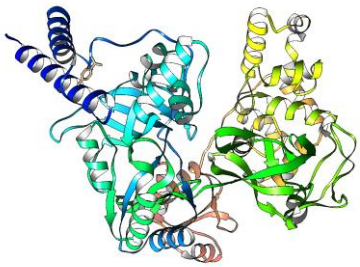	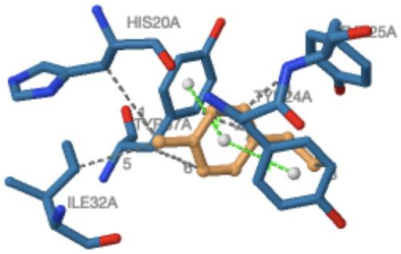
HDOCK LigA- Thymol Docking score: -111.73	AutoDock Vina LigA- Thymol Docking score: -6.2	2D protein–ligand interaction map
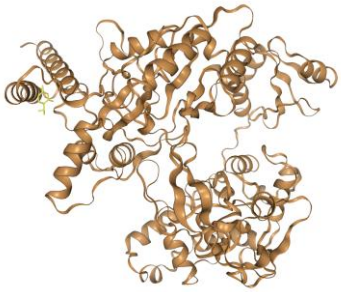	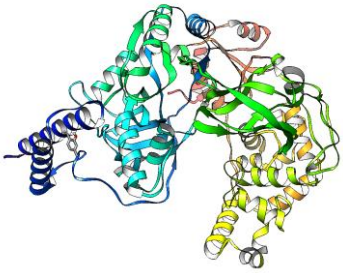	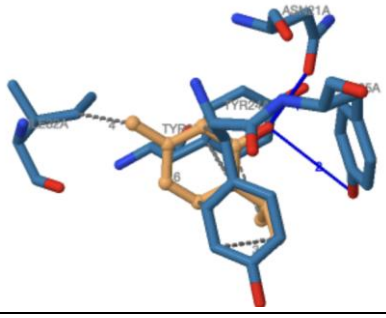

Based on HDOCK docking scores, carvacrol exhibited the strongest binding affinity to LigA (-112.21), followed by thymol (-111.73) and p-cymene (-97.96), while AutoDock Vina results also showed strong interactions with p-cymene (-7.0) and carvacrol (-6.9), highlighting carvacrol's favorable binding in both methods.

This study analyzed LigA-ligand interactions using docking procedures with HDOCK and AutoDock Vina (Trott *et al*., 2010; Nadeem *et al*., 2021), where HDOCK generated 10 optimal models per protein-ligand pair, detailed in Table 18, and AutoDock Vina produced eight models per complex, with docking scores and RMSD values presented in Table 18. The comparison of results from both methods highlighted the binding affinities and potential effects of the ligands on LigA, with negative docking scores prioritized for model selection.

Table 18. Summary of HDOCK docking results for LigA and ligands (Trott *et al*., 2010; Yan *et al*., 2020).

Results of HDOCK		Docking Score	Confidence Score	Ligand rmsd
LigA-Beta-caryophyllene	Model 1	-93.18	0.2430	15.28
	Model 2	-90.40	0.2329	32.58
	Model 3	-89.85	0.2309	11.72
	Model 4	-83.88	0.2104	18.70
	Model 5	-81.73	0.2034	33.10
	Model 6	-80.66	0.1999	31.67
	Model 7	-80.53	0.1995	10.31
	Model 8	-76.87	0.1881	21.71
	Model 9	-76.72	0.1876	29.41
	Model 10	-75.99	0.1854	22.02
Results of AutoDock Vina		Docking Score	RMSD I.b	RMSD u.b
LigA-Beta-caryophyllene	Model 1	-6.7	4.05	6.809
	Model 2	-6.4	3.298	5.173
	Model 3	-5.7	8.583	12.113
	Model 4	-5.6	4.743	8.173
	Model 5	-5.5	10.905	13.567
	Model 6	-5.5	5.123	7.482
	Model 7	-5.4	8.947	12.452
	Model 8	-5.4	10.136	12.923
Results of HDOCK		Docking Score	Confidence Score	Ligand rmsd
LigA- Carvacrol	Model 1	-112.21	0.3196	33.17
	Model 2	-84.59	0.2128	31.76
	Model 3	-80.69	0.2000	12.65
	Model 4	-80.02	0.1979	29.08
	Model 5	-74.00	0.1795	26.71
	Model 6	-73.40	0.1777	19.21
	Model 7	-72.37	0.1747	20.39
	Model 8	-70.89	0.1705	33.39
	Model 9	-70.08	0.1682	15.63
	Model 10	-69.92	0.1678	24.65
Results of AutoDock Vina		Docking Score	RMSD I.b	RMSD u.b
LigA- Carvacrol	Model 1	-6.9	1.764	2.389
	Model 2	-6.3	2.216	4.859
	Model 3	-6.2	1.76	4.408
	Model 4	-6.1	1.148	1.612
	Model 5	-6.0	1.853	2.698
	Model 6	-5.4	2.686	3.955
	Model 7	-4.9	2.305	4.812
	Model 8	-4.8	2.715	5.374

Results of HDOCK		Docking Score	Confidence Score	Ligand rmsd
LigA-Gamma-terpinene	Model 1	-94.55	0.2481	33.02
	Model 2	-68.38	0.1635	11.18
	Model 3	-67.77	0.1618	32.14
	Model 4	-67.70	0.1617	28.78
	Model 5	-63.61	0.1509	31.86
	Model 6	-63.25	0.1499	20.43
	Model 7	-62.70	0.1486	19.07
	Model 8	-61.76	0.1462	24.77
	Model 9	-60.94	0.1442	15.00
	Model 10	-59.63	0.1410	26.93
Results of AutoDock Vina		Docking Score	RMSD I.b	RMSD u.b
LigA-Gamma-terpinene	Model 1	-6.7	0.15	1.592
	Model 2	-6.2	0.872	4.394
	Model 3	-6.1	0.891	4.672
	Model 4	-5.0	1.649	4.903
	Model 5	-4.7	1.726	2.952
	Model 6	-4.2	9.979	11.947
	Model 7	-4.2	10.09	11.994
	Model 8	-4.1	12.801	14.488
Results of HDOCK		Docking Score	Confidence Score	Ligand rmsd
LigA-P-cymene	Model 1	-97.96	0.2610	32.96
	Model 2	-72.59	0.1649	31.97
	Model 3	-68.89	0.1614	28.90
	Model 4	-72.59	0.1614	11.67
	Model 5	-68.89	0.1531	26.73
	Model 6	-63.11	0.1496	20.34
	Model 7	-63.01	0.1493	24.46
	Model 8	-62.54	0.1481	18.89
	Model 9	-61.21	0.1448	15.21
	Model 10	-59.36	0.1403	30.97
Results of AutoDock Vina		Docking Score	RMSD I.b	RMSD u.b
LigA-P-cymene	Model 1	-7.0	0.089	1.537
	Model 2	-6.4	1.349	1.907
	Model 3	-6.4	1.129	4.481
	Model 4	-5.6	1.443	4.742
	Model 5	-4.7	1.753	5.227
	Model 6	-4.5	2.933	5.583
	Model 7	-4.3	9.871	11.788
	Model 8	-4.1	13.061	14.269
Results of HDOCK		Docking Score	Confidence Score	Ligand rmsd
LigA-Thymol	Model 1	-111.73	0.3175	33.23
	Model 2	-84.62	0.2129	32.08
	Model 3	-79.70	0.1969	12.19
	Model 4	-77.06	0.1887	28.08
	Model 5	-73.95	0.1793	30.81
	Model 6	-72.30	0.1745	15.16
	Model 7	-72.12	0.1740	24.61
	Model 8	-70.17	0.1685	10.86
	Model 9	-67.45	0.1610	10.55
	Model 10	-66.63	0.1588	38.80
Results of AutoDock Vina		Docking Score	RMSD I.b	RMSD u.b
	Model 1	-6.2	1.14	4.067

LigA-Thymol	Model 2	-6.2	1.009	1.284
	Model 3	-5.7	1.908	2.768
	Model 4	-5.6	1.735	2.446
	Model 5	-5.0	1.732	4.576
	Model 6	-4.7	1.578	4.611
	Model 7	-4.4	13.157	14.546
	Model 8	-4.3	12.791	13.644

The PLIP (Protein-Ligand Interaction Profiler) tool was used to analyze the interactions between OmpA, LigA, and their ligands, identifying interaction types and specific amino acids involved, with details on distances, angles, and donor/acceptor atoms presented in Tables15, 17, 19 and 20 (https://plip-tool.biotec.tu-dresden.de/plip-web/plip/index).

Table 19. Results of OmpA-ligand interactions (https://plip-tool.biotec.tu-dresden.de/plip-web/plip/index).

Ligand	Interaction type	Protein residue	Residue number	Distance (Å)
Beta-caryophyllene	Hydrophobic	ASN	272	3.47
Beta-caryophyllene	Hydrophobic	ARG	276	3.72
Beta-caryophyllene	Hydrophobic	TRP	312	3.72
Carvacrol	Hydrophobic	GLU	68	3.51
Carvacrol	Hydrophobic	TYR	105	2.50
Carvacrol	Hydrophobic	THR	107	2.95
Carvacrol	Hydrophobic	PHE	158	3.47
Carvacrol	Hydrogen bond	TYR	105	2.37
Carvacrol	Hydrogen bond	ASN	191	3.63
Carvacrol	π–π stacking	PHE	158	4.37
Gamma-terpinene	Hydrophobic	LEU	55	3.55
Gamma-terpinene	Hydrophobic	TYR	132	3.84
Gamma-terpinene	Hydrophobic	PHE	134	3.59
Gamma-terpinene	Hydrophobic	VAL	137	3.72
Gamma-terpinene	Hydrophobic	GLU	179	3.90
Gamma-terpinene	Hydrophobic	PHE	181	3.75
p-cymene	Hydrophobic	LEU	55	3.02
p-cymene	Hydrophobic	TYR	130	2.87
p-cymene	Hydrophobic	TYR	132	3.22
p-cymene	Hydrophobic	TYR	132	2.85
p-cymene	Hydrophobic	PHE	134	3.11
p-cymene	Hydrophobic	PHE	134	3.99
p-cymene	Hydrophobic	GLU	146	3.10
p-cymene	Hydrophobic	GLU	179	3.03
p-cymene	Hydrophobic	PHE	181	2.89
p-cymene	π–π stacking	TYR	132	4.95
Thymol	Hydrogen bond	GLU	68	4.00
Thymol	Hydrophobic	TYR	105	3.07
Thymol	Hydrophobic	THR	107	3.72
Thymol	Hydrophobic	PHE	158	3.69
Thymol	Hydrophobic	PHE	158	3.43
Thymol	Hydrophobic	PHE	158	3.81
Thymol	Hydrophobic	PHE	158	3.17
Thymol	Hydrophobic	ARG	160	3.74
Thymol	Hydrogen bond	TYR	105	2.22

Table 20. Results of LigA-ligand interactions (https://plip-tool.biotec.tu-dresden.de/plip-web/plip/index).

Ligand	Interaction type	Protein residue	Residue number	Distance (Å)
Beta-caryophyllene	Hydrophobic	LEU	84	3.78
Beta-caryophyllene	Hydrophobic	TYR	228	3.29
Beta-caryophyllene	Hydrophobic	TRP	312	3.30
Carvacrol	Hydrophobic	HIS	20	3.49
Carvacrol	Hydrophobic	TYR	24	3.32
Carvacrol	Hydrophobic	TYR	24	3.75
Carvacrol	Hydrophobic	TYR	24	3.38
Carvacrol	Hydrophobic	TYR	24	3.71
Carvacrol	Hydrophobic	TYR	25	3.74
Carvacrol	Hydrophobic	ILE	32	3.56
Carvacrol	Hydrophobic	TYR	37	3.51
Carvacrol	Hydrogen bond	TYR	32	2.33
Carvacrol	π–π stacking	TYR	37	3.99
Gamma-terpinene	Hydrophobic	HIS	20	3.41
Gamma-terpinene	Hydrophobic	TYR	24	3.43
Gamma-terpinene	Hydrophobic	TYR	24	3.86
Gamma-terpinene	Hydrophobic	TYR	25	3.46
Gamma-terpinene	Hydrophobic	ILE	32	3.76
Gamma-terpinene	Hydrophobic	TYR	37	3.82
Gamma-terpinene	Hydrophobic	TYR	37	3.64
Gamma-terpinene	Hydrophobic	TYR	37	3.93
Gamma-terpinene	π–π stacking	TYR	24	3.98
Gamma-terpinene	π–π stacking	TYR	37	3.88
p-cymene	Hydrophobic	HIS	20	3.56
p-cymene	Hydrophobic	TYR	24	3.38
p-cymene	Hydrophobic	TYR	24	3.90
p-cymene	Hydrophobic	TYR	25	3.66
p-cymene	Hydrophobic	ILE	32	3.62
p-cymene	Hydrophobic	TYR	37	3.65
p-cymene	Hydrophobic	TYR	37	3.67
p-cymene	π–π stacking	TYR	24	4.01
p-cymene	π–π stacking	TYR	37	3.91
Thymol	Hydrophobic	TYR	24	3.39
Thymol	Hydrophobic	TYR	24	3.32
Thymol	Hydrophobic	ILE	24	3.51
Thymol	Hydrophobic	TYR	32	3.21
Thymol	Hydrophobic	TYR	37	3.35
Thymol	Hydrophobic	TYR	37	3.88
Thymol	Hydrophobic	TYR	37	3.72
Thymol	Hydrophobic	TYR	37	3.20
Thymol	Hydrogen bond	ASN	21	2.57
Thymol	Hydrogen bond	TYR	25	3.91

Determination of MIC of O. *vulgare* Essential Oil Against *A. baumannii* Strains

It was determined that the OVEOs had an antibacterial effect on *A. baumannii* strains, and the MIC% (v/v) value was between 3.13 and 0.39 (Table 21).

Table 21. MIC activities of *Origanum vulgare* essential oil against *A. baumannii* strains

Essential oils	MIC% (v/v)			
	A. baumannii strains			
	Ab OR792201	Ab OR792202	Ab OR792203	Ab OR792204
OVEO	0.003125	0.0015625	0.003125	0.0015625

DISCUSSION and CONCLUSION

Carvacrol, found in oregano and thyme essential oils, has shown significant antimicrobial properties. Mechmechani *et al*. (Mechmechani *et al*., 2022) demonstrated that carvacrol reduced *Pseudomonas aeruginosa* biofilm below detection levels within 15 minutes. It has also been effective against multidrug-resistant *Klebsiella pneumoniae*, with low MIC and MBC values (130-260 mg/L) (de Souza *et al*., 2021). Carvacrol disrupts the bacterial cell membrane, making it more permeable, which indirectly affects outer membrane proteins like OmpA, potentially reducing their ability to interact with host cells. While there is no direct inhibition of LigA by carvacrol, oxidative stress and membrane damage may indirectly influence processes with DNA replication. In a study, it was observed that the anti-biofilm effects of sub-MIC carvacrol on *A. baumannii* (Pakzad *et al*., 2024).

P-cymene, found in essential oils, increases membrane permeability by disrupting lipid components. It has been shown to have lower antimycobacterial activity than carvacrol and thymol, but it can destabilize outer membrane proteins like OmpA, weakening biofilm formation. Although no direct inhibition of LigA has been reported, increased membrane permeability can indirectly affect DNA replication and repair processes (Andrade *et al*., 2015).

Thymol, a phenolic compound with a structure similar to carvacrol, also disrupts bacterial membrane lipids, inhibiting bacterial metabolism and biofilm formation. While there is no direct data on thymol binding to LigA, its membrane-damaging effects may negatively impact DNA replication (da Silva Cirino *et al*., 2024). Gamma-terpinene, a lipophilic compound, increases membrane permeability and destabilizes OmpA, weakening biofilm formation. Its oxidative effects may indirectly disrupt DNA replication processes (da Silva Cirino *et al.,* 2024). Beta-caryophyllene, found in black pepper and cloves, disrupts membrane permeability and supports immune responses. While it may destabilize OmpA and affect DNA replication indirectly, no direct interaction with LigA has been observed (Prerna *et al.,* 2024).

OmpA is a protein with multifunctional functions found in the outer membrane of gram-negative bacteria. OmpA plays an important role in the pathogenesis of bacterial infections (Heidarian *et al.,* 2024). LigA is an enzyme required for DNA replication and repair in bacteria. It differs from eukaryotic DNA ligases in its NAD^+ dependency. LigA is a specific antibiotic target because it is found only in bacteria. Inhibition of LigA can prevent DNA repair and replication, leading to bacterial death (Sugawara and Nikaido, 2012). Experimental molecules such as Cyclidine derivatives, identified as OmpA inhibitors, can disrupt the stability of the outer membrane of bacteria. Such inhibitors are under development in laboratory studies. Molecules that disrupt the function of OmpA can enhance the effect of other antibiotics by increasing the permeability of the outer membrane (Vaishnav *et al.,* 2024). LigA inhibitors such as Rifamycin derivatives, Pyridopyrimidine derivatives, and the natural compound Plumbagin offer alternatives to traditional antibiotics in the treatment of bacterial infections. The specificity of the NAD^+-dependent mechanism to bacteria increases the possibility of selective toxicity (Ma *et al*., 2024; Pals *et al.,* 2024).

The docking analyses and MIC results were evaluated in a complementary manner. Docking scores provide insights into the potential molecular interactions of individual compounds with specific protein targets, such as OmpA and LigA, whereas MIC values reflect the overall antibacterial activity of the essential oil mixtures, which may involve multiple mechanisms of action. In this study, thymol and carvacrol exhibited the highest docking scores in HDOCK

analyses, indicating favorable shape complementarity and binding site localization, while AutoDock Vina highlighted γ-terpinene and p-cymene as energetically favorable ligands depending on the target protein. Experimentally, Origanum vulgare essential oil showed antibacterial activity against A. baumannii strains with MIC values ranging from 0.39% to 3.13% (v/v). The observed antibacterial effect is likely not solely dependent on high-affinity binding to a single protein but rather reflects synergistic and membrane-disruptive effects of the essential oil components. Compounds such as thymol, carvacrol, and p-cymene are known to increase membrane permeability, which may enhance intracellular access and indirectly affect proteins involved in virulence and DNA replication. Therefore, while docking scores support potential target interactions, the MIC results highlight the importance of multi-target and physicochemical mechanisms contributing to the overall antimicrobial activity.

To better interpret the docking results in the context of the experimentally observed antibacterial activity, the potential mechanisms of action of the essential oil components were further evaluated based on previously reported literature. In an experimental study, carvacrol was reported to exhibit a high affinity for hydrophobic phases and to integrate into liposomal membranes, leading to membrane expansion, as reflected by its high partition coefficients in octanol–water and liposome–buffer systems. This effect was shown to increase in a concentration-dependent manner, with maximal membrane expansion observed beyond a certain threshold. In the same study, comparative analyses with structurally related compounds such as thymol, p-cymene, menthol, and carvacrol methyl ester demonstrated that carvacrol destabilizes the cytoplasmic membrane and acts as a proton exchanger, thereby reducing the transmembrane pH gradient. The resulting collapse of the proton motive force and depletion of ATP pools were shown to ultimately trigger cell death, indicating that the antibacterial activity of lipophilic essential oil components such as thymol, carvacrol, and p-cymene primarily relies on disruption of the bacterial cell membrane integrity (Ultee *et al*., 2002).

In another study, the minimum inhibitory concentrations (MICs) of oregano essential oil (OEO) and its two major components, thymol and carvacrol, were evaluated against *Pseudomonas aeruginosa* and *Staphylococcus aureus* strains, and the mechanisms of action of these compounds were investigated. The findings demonstrated that the combined use of thymol and carvacrol at appropriate ratios could reproduce the complete antibacterial inhibition observed for oregano essential oil. This effect was attributed to damage to the bacterial cell membrane integrity, leading to increased membrane permeability and subsequent disruption of pH homeostasis and inorganic ion balance. These results support that the antibacterial activities of thymol and carvacrol are primarily membrane-targeted and that synergistic interactions among essential oil components play a critical role (Lamber *et al*., 2001). In another experimental study, the role of membrane disruption in the bactericidal activity of plant-derived aromatic essential oil compounds, including eugenol, carvacrol, and cinnamaldehyde, was investigated. The study demonstrated that eugenol and carvacrol rapidly increased propidium iodide uptake in *Escherichia coli*, *Listeria monocytogenes*, and *Lactobacillus sakei* cells, indicating an increase in cell membrane permeability. In addition, treatments with eugenol and carvacrol were reported to cause a reduction in cell viability, rapid depletion of intracellular ATP levels, and ATP release. These findings support the possibility that these compounds may exhibit ATPase inhibitory activity and that this effect is associated with a membrane disruption–related mechanism (Gill *et al*., 2006). P-cymene is a monocyclic monoterpene containing a benzene ring and is recognized as a biosynthetic precursor of carvacrol. It has been reported to increase the permeability of the cytoplasmic membrane to adenosine triphosphate (ATP), thereby influencing cellular energy homeostasis (Ben Arfa *et al*., 2006; Azizi *et al*., 2020). Several studies have shown that p-cymene exhibits antimicrobial activity when applied alone and can also enhance the antibacterial efficacy of other compounds when used in combination (Baginska *et al*.,2023; Pinna *et al*., 2022; Rattanachaikunsopon *et al*., 2010; Bourhia *et al*., 2023). This potentiating effect is mainly attributed to its high affinity for microbial membranes, where it can disrupt membrane potential and induce membrane expansion and structural

disorder. Moreover, by altering membrane integrity, p-cymene may facilitate the intracellular penetration of other antimicrobial agents, indirectly amplifying their activity. Collectively, these findings suggest that p-cymene functions not as a strong direct inhibitor but rather as a membrane-permeabilizing and synergistic compound that supports the overall antimicrobial effect (Baginska *et al*.,2023; Pinna *et al*., 2022; Rattanachaikunsopon *et al*., 2010; Bourhia *et al*., 2023). In this context, the interactions observed between these compounds and OmpA and LigA in docking analyses are more likely to reflect secondary or indirect effects rather than direct enzymatic inhibition. Disruption of membrane integrity may alter the functional environment of outer membrane and DNA replication–associated proteins, thereby indirectly influencing OmpA- and LigA-related processes.

In this study, the interactions between the OmpA and LigA proteins and the compounds carvacrol, p-cymene, thymol, gamma-terpinene, and beta-caryophyllene were investigated. The homology models generated for both LigA and OmpA exhibited high quality, as indicated by favorable PROCHECK and ERRAT values, demonstrating stable and reliable protein structures. Docking analyses revealed that thymol and carvacrol achieved the highest binding scores in HDOCK simulations for both OmpA and LigA, reflecting favorable shape complementarity and accurate binding site localization. In this study, AutoDock Vina results were primarily considered during the model selection process due to their ability to estimate binding free energies. AutoDock Vina enables the identification of the most energetically favorable protein-ligand complexes by evaluating the thermodynamic feasibility of ligand–protein interactions. In contrast, HDOCK analyses were employed to validate binding site localization and to assess the spatial positioning of ligands on the protein surface. The shape complementarity-based approach of HDOCK helped confirm the proper placement of ligands within active or potential binding pockets. The combined use of both methods allowed a comprehensive evaluation of both spatial compatibility and binding energetics, thereby enhancing the overall reliability of the results. Based on AutoDock Vina binding energy calculations, gamma-terpinene (-5.6 kcal/mol) and p-cymene (-5.4 kcal/mol) exhibited the most favorable binding energies for OmpA, and these complexes were therefore selected as representative OmpA–ligand models for further analysis. For LigA, AutoDock Vina results indicated that p-cymene (-7.0 kcal/mol) and carvacrol (-6.9 kcal/mol) showed the lowest binding free energies among the tested compounds. Accordingly, these OmpA- and LigA-ligand complexes were selected as the most energetically favorable models for subsequent structural and interaction analyses.

Declaration of Conflicting Interests and Ethics

The authors declare no conflict of interest. This research study complies with research and publishing ethics. The scientific and legal responsibility for manuscripts published in IJSM belongs to the authors.

Data Availability Statement

We utilized the pkCSM platform, which employs machine learning models to predict key ADMET properties for small molecules. This platform offers 28 different regression and classification models trained on extensive datasets to predict absorption, distribution, metabolism, excretion, and toxicity (ADMET) descriptors. The ligands (Carvacrol, Beta-caryophyllene, Gamma-terpinene, Thymol, and P-cymene) were sourced from PubChem (PubChem CID numbers: Carvacrol [10364], Beta-caryophyllene [5281515], Gamma-terpinene [7461], Thymol [6989], P-cymene [7643]) and these IDs were used in pkCSM and Swiss ADMET web servers. Protein sequences for OmpA and LigA were obtained from NCBI in FASTA format. The three-dimensional structures of these proteins were generated via homology modeling using online tools including Swiss-Model, GalaxyWEB, and AlphaFold. The obtained .pdb files for OmpA and LigA were used for homology modeling using Swiss-Model (model IDs for LigA: B0V8E4.1.A, 5tt5.1.A, 2owo.1.D, 1dgs.2.A, 1ta8.1.A, and model IDs for OmpA: 7q5c.1.A, 2mlh.1.A, 3nb3.1.A, 3td5.3.B, A3M8K2.1.A. The ligands (Carvacrol, Beta-caryophyllene, Gamma-terpinene, Thymol, and P-cymene) were sourced from PubChem (PubChem CID numbers: Carvacrol [10364], Beta-caryophyllene [5281515], Gamma-terpinene [7461], Thymol [6989], P-cymene [7643) and prepared for docking studies. Active sites on the proteins were predicted based on

evolutionary conservation analysis. The Consurf web server was used to identify conserved regions that are likely involved in ligand binding and catalytic functions. Additionally, the UCSF Chimera software was used to visualize the hydrophobic and hydrophilic regions in the 3D protein models. The proteins were prepared using UCSF Chimera (version 1.15) by removing water molecules, salts, and native ligands, followed by docking simulations. The docking results were analyzed, and the best models were selected based on docking scores and interaction analysis. The antimicrobial activity of Origanum vulgare essential oil was evaluated against four clinical isolates of Acinetobacter baumannii (Ab1, Ab2, Ab3, and Ab4) using the Minimum Inhibitory Concentration (MIC) method. The MIC values were determined following the Clinical and Laboratory Standards Institute (CLSI) guidelines.

Funding

The authors declare that no funds, grants, or other support were received during the preparation of this manuscript.

Authorship Contribution Statement

G.K.K.: Investigation, Methodology, Supervision, Material preparation, data collection and analysis, draft. **T.K.:** Methodology, Material preparation, data collection and analysis, draft. **A.B.A.:** Methodology, Material preparation, data collection and analysis, draft. **S.E.K.:** Investigation, Methodology, draft. **M.K.:** Investigation, Methodology, draft.

Orcid

Gizem Köprülülü Kücük https://orcid.org/0000-0001-6667-4532
Tuğba Kaman https://orcid.org/0000-0002-5885-0193
Ahmed Badri Abed https://orcid.org/0000-0002-7803-7917
Safiye Elif Korcan https://orcid.org/0000-0001-7875-5516
Muhsin Konuk https://orcid.org/0000-0002-6651-718X

REFERENCES

Alomari, A., Gowland, R., Southwood, C., Barrow, J., Bentley, Z., Calvin-Nelson, J., Kaminski, A., LeFevre, M., Callaghan, A.J., Vincent, H.A., Gowers, D.M. (2021). Identification of Novel Inhibitors of *Escherichia coli* DNA Ligase (LigA). *Molecules*, *26*(9), 2508. https://doi.org/10.3390/molecules26092508

Andrade-Ochoa, S., Nevárez-Moorillón, G.V., Sánchez-Torres, L.E., Villanueva-García, M., Sánchez-Ramírez, B.E., Rodríguez-Valdez, L.M., & Rivera-Chavira, B.E. (2015). Quantitative structure–activity relationship of molecules constituent of different essential oils with antimycobacterial activity against *Mycobacterium tuberculosis* and *Mycobacterium bovis*. BMC Complementary and Alternative Medicine, 15, 1-11. https://doi.org/10.1186/s12906-015-0858-2

Armon, A., Graur, D., & Ben-Tal, N. (2001). ConSurf: An algorithmic tool for the identification of functional regions in proteins by surface mapping of phylogenetic information. *Journal of Molecular Biology*, *307*(1), 447-463. https://doi.org/10.1006/jmbi.2000.4474

Avola, R., Granata, G., Geraci, C., Napoli, E., Graziano, A.C.E., Cardile, V. (2020). Oregano (*Origanum vulgare* L.) essential oil provides anti-inflammatory activity and facilitates wound healing
in a human keratinocytes cell model. *Food and Chemical Toxicology, 144*, 111586. https://doi.org/10.1016/j.fct.2020.111586

Ayoub Moubareck, C., & Hammoudi Halat, D. (2020). Insights into *Acinetobacter baumannii*: A Review of Microbiological, Virulence, and Resistance Traits in a Threatening Nosocomial Pathogen. *Antibiotics*, *9*(3), 119. https://doi.org/10.3390/antibiotics9030119

Azizi, Z.; Salimi, M.; Amanzadeh, A.; Majelssi, N.; Naghdi, N. (2020). Carvacrol and Thymol Attenuate Cytotoxicity Induced by Amyloid β25-35 via Activating Protein Kinase C and Inhibiting Oxidative Stress in PC12 Cells. *Iran Biomedical Journal*, *24*, 243-250. https://doi.org/10.29252/ibj.24.4.243

Baginska, S., Gologniko, A., Swislocka, R., Lewandowski, W. (2023). Monoterpenes as medicinal agents: Exploring the pharmaceutical potential of p-cymene, p-cymenene, and γ-terpinene. *Acta Poloniae Pharmaceutica- Drug Research, 80*, 879-892. https://doi.org/10.32383/appdr/178242

Ben Arfa, A., Combes, S., Preziosi-Belloy, L., Gontard, N., Chalier, P. (2006). Antimicrobial activity of carvacrol related to its chemical structure. *Letters Apply Microbiology, 43*, 149-154. https://doi.org/10.1111/j.1472-765X.2006.01938.x

Bourhia, M., Alyousef, A.A., Doumane, G., Saghrouchni, H., Giesy, J.P., Ouahmane, L., Gueddari, F.E., Al-Sheikh, Y.A., Aboul-Soud, M.A.M. (2023). Volatile Constituents in Essential Oil from Leaves of Withania adpressa Coss. Ex Exhibit Potent Antioxidant and Antimicrobial Properties against Clinically-Relevant Pathogens. *Molecules, 28*, 2839. https://doi.org/10.3390/molecules28062839.

Clinical and Laboratory Standards Institute. (2012). Methods for dilution antimicrobial susceptibility tests for bacteria that grow aerobically; approved standard (9th ed., CLSI document M07-A9). CLSI.

Colovos, C., & Yeates, T.O. (1993). Verification of protein structures: Patterns of nonbonded atomic interactions. *Protein Science, 2*(9), 1511-1519. https://doi.org/10.1002/pro.5560020916

da Silva Cirino, I.C., de Santana, C.F., Vasconcelos Rocha, I., de Souza, L.I.O., Silva, M.V., Bressan Queiroz de Figueiredo, R.C., Coutinho H.D.M., & Leal-Balbino, T.C. (2024). The Combinatory Effects of Essential Oil from *Lippia macrophylla* oil on multidrug-resistant Acinetobacter baumannii clinical isolates. *Chemistry & Biodiversity*, *21*(10), e202400537. https://doi.org/10.1002/cbdv.202400537

De Souza, G.H.D.A., dos Santos Radai, J.A., Mattos Vaz, M.S., Esther da Silva, K., Fraga, T.L., & Barbosa, L. (2021). In vitro and in vivo antibacterial activity assays of carvacrol: A candidate for the development of innovative treatments against KPC-producing *Klebsiella pneumoniae*. *PLoS ONE, 16(*2). https://doi.org/10.1371/journal.pone.0246003

Erol, M., Çelik, I., & Kuyucuklu, G. (2021). Synthesis, molecular docking, molecular dynamics, DFT, and antimicrobial activity studies of 5-substituted-2-(p-methylphenyl) benzoxazole derivatives. *Journal of Molecular Structure*, 1234. https://doi.org/10.1016/j.molstruc.2021.130151

Fikry, S., Khalil, N., & Salama, O., (2010). Chemical profiling, biostatic and biocidal dynamics of *Origanum vulgare* L. essential oil. *AMB Express, 9*, 41. https://doi.org/10.1186/s13568-019-0764-y

Filimonov, D.A., Lagunin, A.A., Gloriozova, T.A., Rudik, A.V., Druzhilovskii, D.S., Pogodin, P.V., & Poroikov, V.V. (2014). Prediction of the biological activity spectra of organic compounds using the PASS online web resource. *Chemistry of Heterocyclic Compounds, 50*(3), 444 457. https://doi.org/10.1007/s10593-014-1496-1.

Gill, A.O., Holley, R.A. (2006). Disruption of Escherichia coli, Listeria monocytogenes and Lactobacillus sakei cellular membranes by plant oil aromatics, *International Journal of Food Microbiology*, *108(*1), 1-9. https://doi.org/10.1016/j.ijfoodmicro.2005.10.009

Heidarian, S., Kachoie, M.A., Mousavi-Fard, S., & Moattar, F. (2024). Evaluating the chemical composition and antibacterial and antioxidant effects of the essential oil of *Melissa officinalis* L. *Pakistan Journal of Zoology*. DOI: https://dx.doi.org/10.17582/journal.pjz/20240309051129.

Iyer, R., Moussa, S.H., Durand-Reville, T.F., Tommasi, R. & Miller, A. (2017). *Acinetobacter baumannii* OmpA is a selective antibiotic permeant porin. *ACS Infection Diseases, 4*, 373-381. https://doi.org/10.1021/acsinfecdis.7b00168

Jumper, J., Evans, R., Pritzel, A., Green, T., Figurnov, M., Ronneberger, O., & Hassabis, D. (2021). Highly accurate protein structure prediction with AlphaFold. *Nature, 596*(7873), 583-589. https://doi.org/10.1038/s41586-021-03819-2

Ko, J., Park, H., Heo, L., & Seok, C. (2012). GalaxyWEB server for protein structure prediction and refinement. *Nucleic Acids Research, 40*(W1), W294-W297. https://doi.org/10.1093/nar/gks493

Lambert, R.J.W., Skandamis, P.N., Coote, P.J., Nychas, G.J.E. (2001). A study of the minimum inhibitory concentration and mode of action of oregano essential oil, thymol, and carvacrol, *Journal of Applied Microbiology*, *91*, 453-462, https://doi.org/10.1046/j.1365-2672.2001.01428.x

Li, Y., He, L., Xue, Z., Liang, Y., Jiang, J., Wei, Y., Li, H., He, H., Li, R. (2025). Antimicrobial activity of *Origanum vulgare* L. essential oil and its effects on fungal gene expression. PLoS One, 20(8).

Lombrea, A., Antal, D., Ardelean, F., Avram, S., Pavel, I Z., Vlaia, L., & Danciu, C. (2020). A recent insight regarding the phytochemistry and bioactivity of *Origanum vulgare* L. essential oil. *International Journal of Molecular Sciences, 21*(24), 9653. https://doi.org/10.3390/ijms21249653.

Ma, X., Li, H., Ji, J., Zeng, L., Tang, M., Lei, C., & Li, H. (2024). Overexpression of outer membrane protein A (OmpA) increases aminoglycoside sensitivity in mycobacteria. *BMC Microbiology*, *24*(1), 472. https://doi.org/10.1186/s12866-024-03632-7

Man, A., Santacroce, L., Jacob, R., Mare, A., & Man, L. (2019). Antimicrobial activity of six essential oils against a group of human pathogens: A comparative study. *Pathogens, 8*(3), 108. https://doi.org/10.3390/pathogens8030108

Mechmechani, S., Gharsallaoui, A., Fadel, A., El Omari, K., Khelissa, S., Hamze, M., & Chihib, N.E. (2022). Microencapsulation of carvacrol as an efficient tool to fight Pseudomonas aeruginosa and *Enterococcus faecalis* biofilms. PLoS ONE, 17(7), e0270200. https://doi.org/10.1371/journal.pone.0270200

Meier, T.I., Yan, D., Peery, R.B., McAllister, K.A., Zook, C., Peng, S.B., Zhao, G. (2008). Identification and characterization of an inhibitor specific to bacterial NAD+-dependent DNA ligases. *FEBS Journal, 275*(21):5258-71. https://doi.org/10.1111/j.1742-4658.2008.06652.x

Meng, X.Y., Zhang, H.X., Mezei, M., & Cui, M. (2011). Molecular docking: a powerful approach for structure based drug discovery. *Current Computer Aided Drug Design, 7*, 146-157. https://doi.org/10.2174/157340911795677602

Mills, S.D., Eakin, A.E., Buurman, E.T., Newman, J.V., Gao, N., Huynh, H., Johnson, K.D., Lahiri, S., Shapiro, A.B., Walkup, G.K., Yang, W., Stokes, S.S. (2011). Novel bacterial NAD+-dependent DNA ligase inhibitors with broad-spectrum activity and antibacterial efficacy in vivo. *Antimicrob Agents Chemother, 55*(3), 1088-96. https://doi.org/10.1128/AAC.01181-10

Mortensen, B.L. & Skaar, E.P. (2012). Host–microbe interactions that shape the pathogenesis of *A cinetobacter baumannii* infection. Cell. *Microbiology. 14*, 1336-1344. https://doi.org/10.1111/j.1462-5822.2012.01817.x

Nadeem, A., Ahmed, B., Shahzad, H., Craker, L.E., & Muntean, T. (2021). *Verbascum thapsus* (Mullein) versatile polarity extracts: GC-MS analysis, phytochemical profiling, antibacterial potential and antioxidant activity. *Pharmacognosy Magazine, 13*(51), 1488-1497. https://doi.org/10.5530/pj.2021.13.189

National Center for Biotechnology Information. (2024, November 5). NCBI resources. https://www.ncbi.nlm.nih.gov

National Library of Medicine. (2024, November 5). PubChem compound database. https://pubchem.ncbi.nlm.nih.gov

Nie, D., Hu, Y., Chen, Z., Li, M., Hou, Z., Luo, X., Mao, X., Xue X. (2020). Outer membrane protein A (OmpA) as a potential therapeutic target for *Acinetobacter baumannii* infection. *Journal of Biomedical Science, 27*(1), 26. https://doi.org/10.1186/s12929-020-0617-7

Pakzad, I., Yarkarami, F., Kalani, B. S., Shafieian, M., & Hematian, A. (2024). Inhibitory effects of carvacrol on biofilm formation in colistin heteroresistant *Acinetobacter baumannii* clinical isolates. *Current Drug Discovery Technologies, 21*(1), 119-124. https://doi.org/10.2174/0115701638253395230919112548

Pals, M.J., Lindberg, A., & Velema, W.A. (2024). Chemical strategies for antisense antibiotics. *Chemical Society Reviews, 53*(11), 11303-11320. https://doi.org/10.1039/d4cs00238e

Pettersen, E.F., Goddard, T.D., Huang, C.C., Couch, G.S., Greenblatt, D.M., Meng, E.C., & Ferrin, T.E. (2004). UCSF Chimera: A visualization system for exploratory research and analysis. *Journal of Computational Chemistry, 25*(13), 1605–1612. https://doi.org/10.1002/jcc.20084

Pogue, J.M., Zhou, Y., Kanakamedala, H., & Cai B. (2019). Burden of illness in carbapenem-resistant *Acinetobacter baumannii* infections in US hospitals between 2014 and 2019. *BMC Infection Diseases, 22*. https://doi.org/10.1186/s12879-021-07024-4

Pinna, S., Kunz, C., Halpern, A., Harrison, S.A., Jordan, S.F., Ward, J., Werner, F., Lane, N. A (2022). Prebiotic basis for ATP as the universal energy currency. *PLoS Biology, 20*, e3001437. https://doi.org/10.1371/journal.pbio.3001437

Prerna, P., Chadha, J., Khullar, L., Mudgil, U., & Harjai, K. (2024). A comprehensive review on the pharmacological prospects of terpinen-4-ol: From nature to medicine and beyond. *Fitoterapia, 176*, 106051. https://doi.org/10.1016/j.fitote.2024.106051.

Protein–Ligand Interaction Profiler. (2024, December 15). PLIP web server. https://plip-tool.biotec.tu-dresden.de/plip-web/plip/index

Radi, M.S., SalcedoSora, J.E., Kim, S.H., Sudarsan, S., Sastry, A.V., Kell, D.B., Herrgård, M.J., & Feist, A. M. (2022). Membrane transporter identification and modulation via adaptive laboratory evolution. *Metabolic Engineering, 72*, 376-390. https://doi.org/10.1016/j.ymben.2022.05.004

Rattanachaikunsopon, P., Phumkhachorn, P. (2010). Assessment of factors influencing antimicrobial activity of carvacrol and cymene against Vibrio cholerae in food. *Journal of Bioscience and Bioengineering, 110*, 614-619. https://doi.org/10.1016/j.jbiosc.2010.06.010

Scribano, D., Cheri, E., Pompilio, A. *et al*. Acinetobacter baumannii OmpA-like porins: functional characterization of bacterial physiology, antibiotic-resistance, and virulence. *Communications Biology 7*, 948. https://doi.org/10.1038/s42003-024-06645-0.

Simirgiotis, M.J., Burton, D., Parra, F., López, J., Muñoz, P., Escobar, H., Parra, C. (2020). Antioxidant and Antibacterial Capacities of Origanum vulgare L. Essential Oil from the Arid Andean Region of Chile and its Chemical Characterization by GC-MS. *Metabolites. 10*(10), 414. https://doi.org/10.3390/metabo10100414

Skerniškytė, J. *et al*. (2019). The mutation of conservative Asp268 residue in the peptidoglycan-associated domain of the OmpA protein affects multiple *Acinetobacter baumannii* virulence characteristics. *Molecules 24*, 1972. https://doi.org/10.3390/molecules24101972

Smani, Y., McConnell, M.J., Pachón, J. (2012). Role of fibronectin in the adhesion of *Acinetobacter baumannii* to host cells. PLoS ONE, 7. https://doi.org/10.1371/journal.pone.0033073

Smani, Y., Fàbrega, A., Roca, I., Sánchez-Encinales, V., Vila, J., & Pachón, J. (2014). Role of OmpA in the multidrug resistance phenotype of *Acinetobacter baumannii*. *Antimicrobial Agents Chemother, 58*,1806-1808. https://doi.org/10.1128/AAC.02101-13

Structural Analysis and Verification Server. (2024, December 12). https://saves.mbi.ucla.edu/

Sugawara, E., & Nikaido, H. (2012). OmpA is the principal nonspecific slow porin of Acinetobacter baumannii. *Journal of Bacteriology, 194*(15), 4089-4096. https://doi.org/10.1128/JB.00435-12

SwissADME. (2024, October 20). SwissADME: A free web tool to evaluate pharmacokinetics, drug-likeness, and medicinal chemistry friendliness of small molecules. https://www.swissadme.ch

Tapia-Rodriguez, M.R., Cantu-Soto, E.U., Vazquez-Armenta, F.J., Bernal-Mercado, A.T., & Ayala-Zavala, J.F. (2023). Inhibition of Acinetobacter baumannii biofilm formation by terpenes from Oregano (*Lippia graveolens*) essential oil. *Antibiotics, 12*, 1539. https://doi.org/10.3390/antibiotics12101539

Tiku, V. *et al*. (2021). Outer membrane vesicles containing OmpA induce mitochondrial fragmentation to promote pathogenesis of *Acinetobacter baumannii*. *Scientific Reports. 11*, 618. https://doi.org/10.1038/s41598-020-79966-9

Trott, O., & Olson, A.J. (2010). AutoDock Vina: Improving the speed and accuracy of docking with a new scoring function, efficient optimization, and multithreading. *Journal of Computational Chemistry, 31*(2), 455-461. https://doi.org/10.1002/jcc.21334

Ultee, A., Bennik, M.H.J., Moezelaar, R. (2002). The Phenolic Hydroxyl Group of Carvacrol Is Essential for Action against the Food-Borne Pathogen Bacillus cereus. *Apply Environmental Microbiology, 68*. https://doi.org/10.1128/AEM.68.4.1561-1568.2002

Vaishnav, J., & Ampapathi, R.S. (2024). 1H, 15N, and 13C resonance backbone and side-chain assignments and secondary structure determination of the BRCT domain of Mtb LigA. *Biomolecular NMR Assignments, 18*, 1-5. https://doi.org/10.1007/s12104-024-10175-5

Waterhouse, A., Bertoni, M., Bienert, S., Studer, G., Tauriello, G., Gumienny, R., Heer, F.T., de Beer, T.A.P., Rempfer, C., Bordoli, L., Lepore, R., & Schwede, T. (2018). SWISS-MODEL: Homology modeling of protein structures and complexes. *Nucleic Acids Research, 46*(W1), W296–W303. https://doi.org/10.1093/nar/gky427

Way2Drug. (2024, October 20). PASS online: Prediction of activity spectra for biologically active substances. http://www.way2drug.com/passonline

Yan, Y., Tao, H., He, J., & Huang, S.Y. (2020). The HDOCK server for integrated protein-protein docking. *Nature Protocols, 15*(5), 1829-1852. https://doi.org/10.1038/s41596-020-0312-x